Cell Metabolism

Article

Biological age is increased by stress and restored upon recovery

Graphical abstract

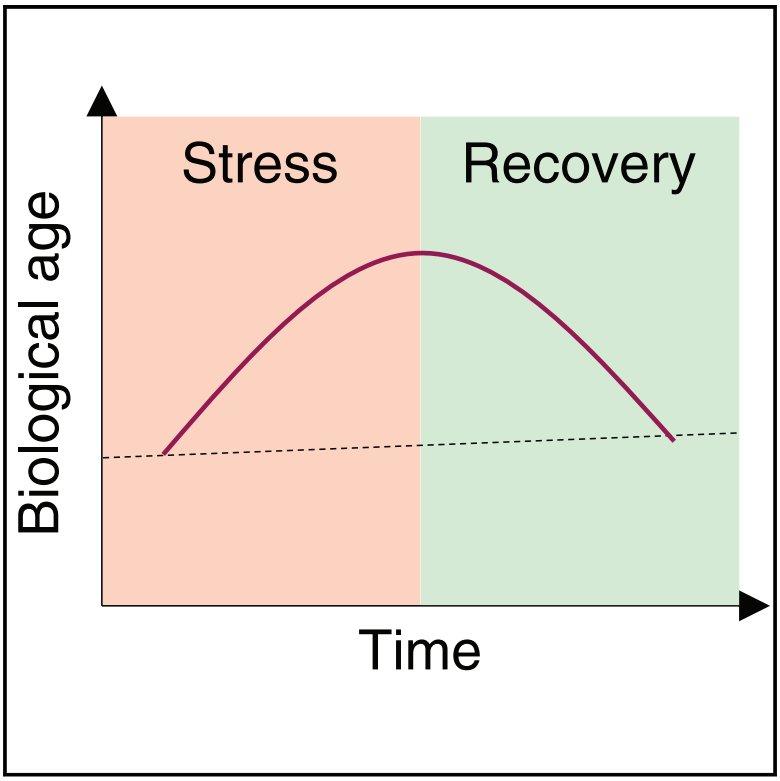

Authors

Jesse R. Poganik, Bohan Zhang, Gurpreet S. Baht, ..., Steve Horvath, James P. White, Vadim N. Gladyshev

Correspondence

james.white@duke.edu (J.P.W.), vgladyshev@rics.bwh.harvard.edu (V.N.G.)

In brief

Poganik et al. analyzed various models of severe stress in mice and humans and found that stress transiently elevates biological age as readout by multiple advanced biomarkers of aging. They demonstrate that biological age is not static, but dynamic.

Highlights

- Biological age undergoes rapid fluctuations in mice and humans
- Severe stress induces increases in biological age that are reversed upon recovery
- Parabiosis, surgery, pregnancy, and COVID-19 transiently elevate biological age
- Biological age recovery rate may predict gerotherapeutics

Poganik et al., 2023, Cell Metabolism *35*, 1–14
May 2, 2023
https://doi.org/10.1016/j.cmet.2023.03.015

CellPress

Please cite this article in press as: Poganik et al., Biological age is increased by stress and restored upon recovery, Cell Metabolism (2023), https://doi.org/10.1016/j.cmet.2023.03.015

Cell Metabolism

CellPress

Article

Biological age is increased by stress and restored upon recovery

Jesse R. Poganik,[1] Bohan Zhang,[1] Gurpreet S. Baht,[2,3] Alexander Tyshkovskiy,[1] Amy Deik,[4] Csaba Kerepesi,[5] Sun Hee Yim,[1] Ake T. Lu,[6,7] Amin Haghani,[6,7] Tong Gong,[8] Anna M. Hedman,[8] Ellika Andolf,[9] Göran Pershagen,[10,11] Catarina Almqvist,[8,12] Clary B. Clish,[4] Steve Horvath,[6,7,13] James P. White,[3,14,*] and Vadim N. Gladyshev[1,4,15,*]

[1]Division of Genetics, Department of Medicine, Brigham and Women's Hospital, Harvard Medical School, Boston, MA 02115, USA
[2]Department of Orthopaedic Surgery, Duke University, Durham, NC 27701, USA
[3]Duke Molecular Physiology Institute, Duke University, Durham, NC 27701, USA
[4]Broad Institute of MIT and Harvard, Cambridge, MA 01241, USA
[5]Institute for Computer Science and Control (SZTAKI), Eötvös Loránd Research Network, Budapest, 1111, Hungary
[6]Department of Human Genetics, David Geffen School of Medicine, University of California, Los Angeles, Los Angeles, CA 90095, USA
[7]Altos Labs, San Diego, CA, USA
[8]Department of Medical Epidemiology and Biostatistics, Karolinska Institutet, Stockholm, Sweden
[9]Department of Clinical Sciences, Division of Obstetrics and Gynaecology, Danderyd Hospital, Karolinska Institutet, Stockholm, Sweden
[10]Institute of Environmental Medicine, Karolinska Institutet, Stockholm, Sweden
[11]Centre for Occupational and Environmental Medicine, Region Stockholm, Stockholm, Sweden
[12]Astrid Lindgren Children's Hospital, Karolinska University Hospital, Stockholm, Sweden
[13]Department of Biostatistics, School of Public Health, University of California, Los Angeles, Los Angeles, CA 90095, USA
[14]Department of Medicine, Duke University School of Medicine, Durham, NC 27701, USA
[15]Lead contact
*Correspondence: james.white@duke.edu (J.P.W.), vgladyshev@rics.bwh.harvard.edu (V.N.G.)
https://doi.org/10.1016/j.cmet.2023.03.015

SUMMARY

Aging is classically conceptualized as an ever-increasing trajectory of damage accumulation and loss of function, leading to increases in morbidity and mortality. However, recent *in vitro* studies have raised the possibility of age reversal. Here, we report that biological age is fluid and exhibits rapid changes in both directions. At epigenetic, transcriptomic, and metabolomic levels, we find that the biological age of young mice is increased by heterochronic parabiosis and restored following surgical detachment. We also identify transient changes in biological age during major surgery, pregnancy, and severe COVID-19 in humans and/or mice. Together, these data show that biological age undergoes a rapid increase in response to diverse forms of stress, which is reversed following recovery from stress. Our study uncovers a new layer of aging dynamics that should be considered in future studies. The elevation of biological age by stress may be a quantifiable and actionable target for future interventions.

INTRODUCTION

The biological age of organisms is thought to steadily increase over the life course. However, it is now clear that biological age is not indelibly linked to chronological age: individuals can be biologically older or younger than their chronological age implies.[1] Moreover, increasing evidence in animal models and humans indicates that biological age can be influenced by disease,[2] drug treatment,[3] lifestyle changes,[4] and environmental exposures,[5] among other factors. Despite the widespread acknowledgment that biological age is at least somewhat malleable, the extent to which biological age undergoes reversible changes throughout life, and the events that trigger such changes remain unknown.

DNA methylation (DNAm) clocks have emerged as the premier tool to assess biological age and begin to answer these questions. Such epigenetic aging clocks were innovated based on the observation that methylation levels of various subsets of CpG sites throughout the genome predictably change over the course of chronological age. First-generation human DNAm clocks[6–8] are constructed using machine learning approaches to build models trained on and designed to predict chronological age. Since the advent of DNAm clocks, both a suite of mouse DNAm clocks[3,9–13] and second-generation human DNAm clocks[14,15] have emerged. Second-generation human DNAm clocks integrate numerous phenotypic measures of aging (and, in some instances, chronological age) to produce a measure of morbidity/mortality risk and biological age. Another recently reported second-generation approach, called DunedinPACE, uses longitudinal phenotypic training data to produce a measure of the rate of biological aging.[16,17] DNAm clocks have excellent predictive ability and are responsive to known anti-aging/lifespan extending interventions

Please cite this article in press as: Poganik et al., Biological age is increased by stress and restored upon recovery, Cell Metabolism (2023), https://doi.org/10.1016/j.cmet.2023.03.015

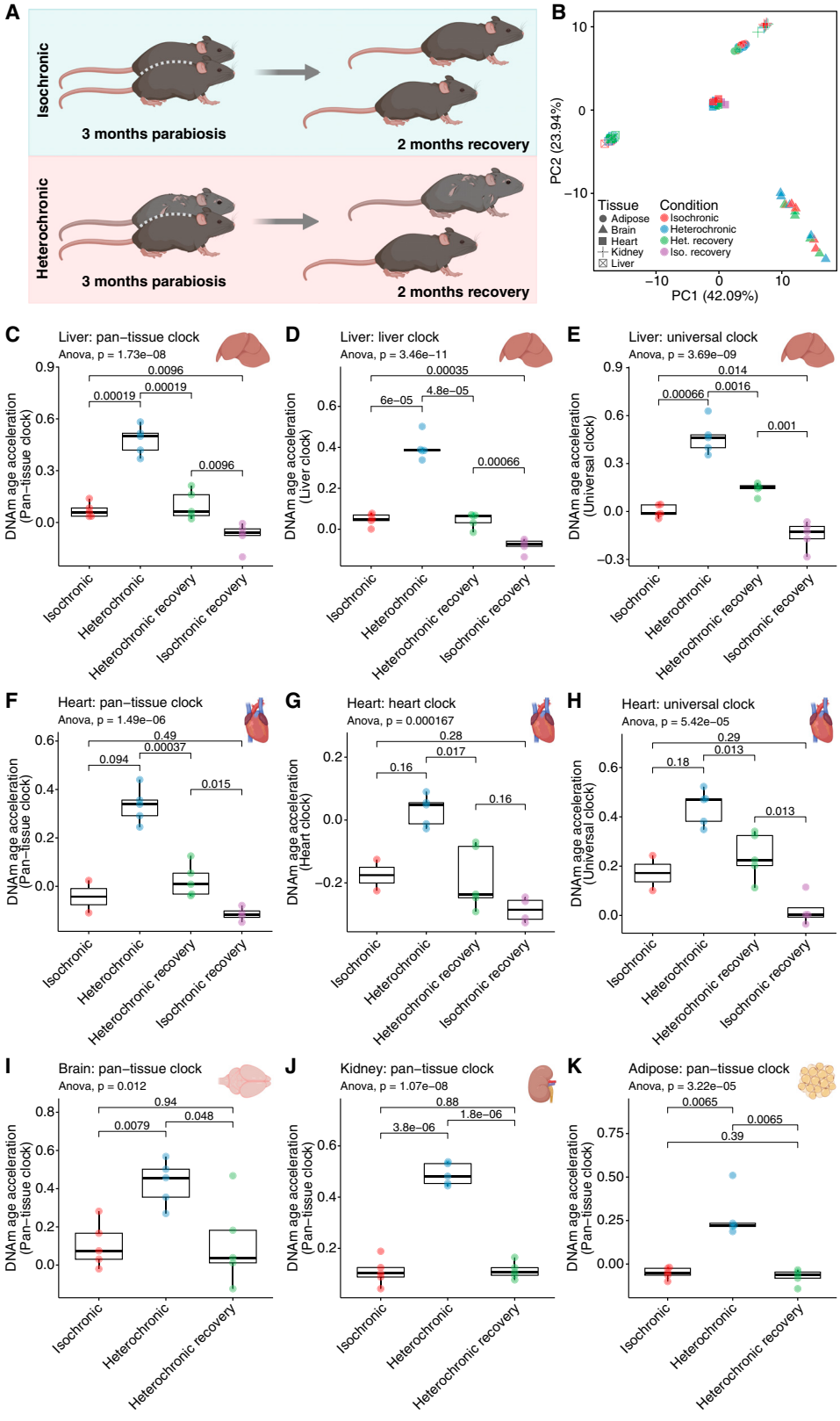

(legend on next page)

Please cite this article in press as: Poganik et al., Biological age is increased by stress and restored upon recovery, Cell Metabolism (2023), https://doi.org/10.1016/j.cmet.2023.03.015

such as caloric restriction.[11] Although mechanistic questions on the nature of DNAm clocks remain, these clocks represent the current gold standard aging biomarker and are now widely utilized in the aging field, including in human clinical trials.[18]

Here, we leverage the power of DNAm clocks in humans and mice to measure reversible biological age changes in response to various stressful stimuli. The use of transcriptomic and metabolomic biomarkers supports this notion. We find that biological age may increase over relatively short time periods in response to stress, but this increase is transient and trends back toward baseline following recovery from stress. Using various stressful events to investigate this question, we further find that second-generation human DNAm clocks give consistent outputs, whereas first-generation human DNAm clocks generally lack the sensitivity to detect transient changes in biological age. Finally, using COVID-19 as a model of severe infectious disease that triggers a reversible increase in biological age, we demonstrate that recovery of biological age following a stress-induced increase is a useful model with which to predict potential anti-aging drugs. Overall, our data suggest that increases in biological age due to stress may be an actionable target for future anti-aging interventions.

RESULTS

Heterochronic parabiosis induces a reversible increase in biological age

We began to examine possible fluctuations in biological age by using a mouse model of heterochronic parabiosis.[19,20] We tested whether the exposure of young mice to aged circulation would induce a change in biological age and whether such a change is reversible. We surgically joined pairs of either 3-month-old mice (isochronic) or a 3-month-old mouse and a 20-month-old mouse (heterochronic). After 3 months of parabiosis, the pairs were separated and allowed to recover for 2 months (Figure 1A). Tissues from the young mice were then analyzed using DNAm clocks, adjusting for chronological age (see STAR Methods). The resulting *DNAm age acceleration* parameter (i.e., chronological-age-adjusted DNAm age) allows for unbiased statistical comparisons between age/treatment groups. This is particularly important for human datasets (below) where samples originate from subjects of diverse chronological ages.

We first analyzed DNAm in liver, heart, brain, kidney, and adipose tissue using the HorvathMammalMethylChip40, which reports the methylation status of approximately 36,000 CpG sites conserved across 159 mammalian species.[21] Principle component analysis of the resulting methylation profiles revealed strong clustering by tissue (Figure 1B). We proceeded to apply a suite of DNAm clocks to our methylation data. Compared with isochronic controls, pan-tissue clocks (i.e., clocks trained on and applicable to multiple tissues[9]), liver-specific clocks, and pan-mammalian clocks trained on methylation data from 185 mammalian species[22] revealed a significant increase in the biological age of livers of heterochronic parabionts (Figures 1C–1E and S1A). Remarkably, the biological age of heterochronic parabionts returned to baseline following detachment and recovery (Figures 1C–1E and S1A). Interestingly, we also observed a small but significant decrease in the biological age of isochronic parabionts following recovery. We attribute this decrease to recovery from the stress of the surgery and parabiosis procedure.

To substantiate these findings, we subjected liver samples from our parabiosis animals to reduced representation bisulfate sequencing (RRBS) and applied several epigenetic clocks trained on RRBS data. We found good agreement with the methylation microarray clocks above. RRBS clocks previously developed by our laboratory[10,11] fully recapitulated the reversible increase in biological age in heterochronic parabionts, as did the Stubbs et al.[12] clock (Figure S1B). Biological ages of isochronic vs. heterochronic parabionts were not significantly different in the Wang et al. clock,[3] although the reversal of biological age in heterochronic parabionts after recovery was significant (Figure S1I). The Thompson et al. clock[13] indicated a significant difference in biological age between isochronic and heterochronic parabionts, but no significant DNAm age reversal following recovery (Figure S1B). Overall, the trends in the data were highly consistent in all clocks across both methylation profiling platforms.

The effects we found in the liver were remarkably consistent across the other tissues examined. The heart (Figures 1F–1H and S1C), brain (Figures 1I and S1D), kidney (Figures 1J and S1E), and adipose (Figures 1K and S1F) all underwent an increase in biological age upon exposure to aged circulation with a return to baseline following detachment. Thus, heterochronic parabiosis induces a systemic increase in the biological age of the young parabiont that is reversed following separation and recovery.

Heterochronic parabiosis perturbs biological age at transcriptomic and metabolomic levels

We next asked whether similar effects could be observed at the level of gene expression and metabolites. Gene expression signatures of aging[23] for liver tissue and mice were significantly positively enriched in heterochronic parabionts; this association

Figure 1. Young mice exposed to aged circulation undergo a reversible increase in biological age

(A) Setup of parabiosis experiment. Young (3 months old) mice were surgically joined with either another young mouse (isochronic) or an old (20 months old) mouse (heterochronic) for 3 months. Following the parabiosis period, mice were separated and allowed to recover for a further 2 months. Tissues from young mice were analyzed using DNAm clocks to assess biological age.

(B) Principal component analysis of methylation data across tissues.

(C–E) DNAm age acceleration results for liver tissue from the HorvathMammalMethyl40 pan-tissue (C), liver (D), and universal pan-mammalian (E) clocks.

(F–H) DNAm age acceleration results for heart tissue using the pan-tissue (F), heart (G), and universal pan-mammalian (H) clocks.

(I–K) Pan-tissue clock DNAm age acceleration results from brain (I), kidney (J), and adipose (K) tissues. p values were calculated with ANOVA and unpaired t tests. Sample sizes: (C–E), n = 6 for isochronic and isochronic recovery, and n = 5 for heterochronic and heterochronic recovery. (F–G), n = 5 for heterochronic and heterochronic recovery, n = 2 for isochronic, and n = 4 for isochronic recovery. (I–K), n = 5 for all conditions.

See also Figure S1.

Please cite this article in press as: Poganik et al., Biological age is increased by stress and restored upon recovery, Cell Metabolism (2023), https://doi.org/10.1016/j.cmet.2023.03.015

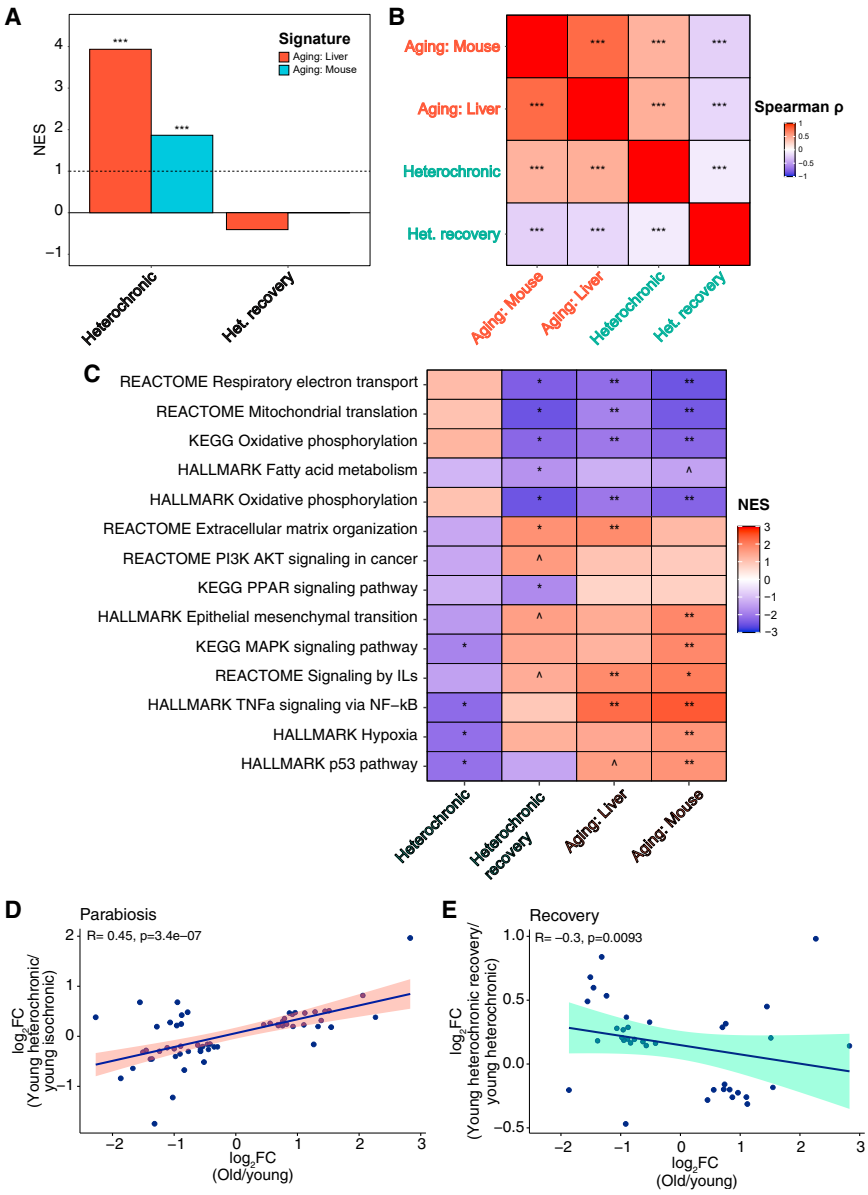

Figure 2. Heterochronic parabiosis reversibly perturbs biological age at the transcriptomic and metabolomic levels

(A) Results of application of aging signatures to sequenced RNA isolated from livers of young heterochronic parabionts upon parabiosis (left) and recovery (right).

(B) Correlation matrix between functions enriched upon heterochronic parabiosis/recovery and those enriched by signatures of aging.

(C) As in (B), but analyzed for enrichment at the pathway level.

(D and E) Correlation of changes in age-related metabolites between aging and heterochronic parabiosis (D) or recovery (E).

Correlation coefficients and p values were calculated with either Spearman correlation (A–C) or Kendall correlation (D and E).

See also Figure S2.

was lost upon recovery (Figure 2A). Similarly, a functional correlation analysis revealed that functions associated with the gene expression profiles of heterochronic parabionts positively correlated with aging profiles constructed for liver tissue and for mice (Figure 2B). Additionally, functional enrichment at the pathway level further confirmed these results—we found a positive correlation between heterochronic parabionts and signatures of aging. This trend was reversed upon recovery (Figure 2C; Table S1).

Metabolomic profiling of livers also yielded consistent results: we observed a significant positive association with age-related metabolites in the heterochronic parabionts (Figures 2D and S2) and a significant inverse association upon recovery (Figure 2E). Overall, these results demonstrate that heterochronic parabiosis induces a transient increase in biological age that manifests at the DNAm, transcriptomic, and metabolomic levels.

Trauma surgery reversibly increases the biological age of elderly patients

Having demonstrated that a transient increase in biological age can be experimentally induced, we sought to identify "natural" situations that similarly cause a reversible change in biological age. Given the links between chronic stress and accelerated biological age,[24,25] we hypothesized that an acute, highly stressful health event might induce such a change. To test this hypothesis, we examined DNAm of blood samples from elderly patients undergoing major surgery.[26] Blood from these patients was taken at three points: (1) immediately before surgery, (2) the morning after surgery, and (3) 4–7 days post-surgery, before discharge from the hospital. Using second-generation human DNAm clocks (DNAmPhenoAge,[14] DNAmGrimAge,[15] and DunedinPACE[17]), we found a significant increase in biological age markers of patients undergoing emergency surgical repair of a traumatic hip fracture. Remarkably, this increase occurred in under 24 h, and biological age returned to baseline 4–7 days post-surgery (Figures 3A–3C). Interestingly, two other non-trauma surgeries did not produce this effect. Patients undergoing elective hip surgery showed an overall increase in biological age markers following surgery, approaching an age acceleration of 0 (or a DunedinPoAm score of just over 1) by the end of their hospitalization (Figures 3D–3F). We note that these patients started at a lower biological age relative to emergency patients (around −5 age acceleration for DNAmPhenoAge and DNAmGrimAge, and 1 for DunedinPoAm), likely reflecting the selection of otherwise healthy surgical candidates and preoperative preparation for a planned surgery.[27] Finally, patients undergoing elective colorectal surgery showed no significant changes in biological age markers over the course of their care (Figures 3G–3I).

Please cite this article in press as: Poganik et al., Biological age is increased by stress and restored upon recovery, Cell Metabolism (2023), https://doi.org/10.1016/j.cmet.2023.03.015

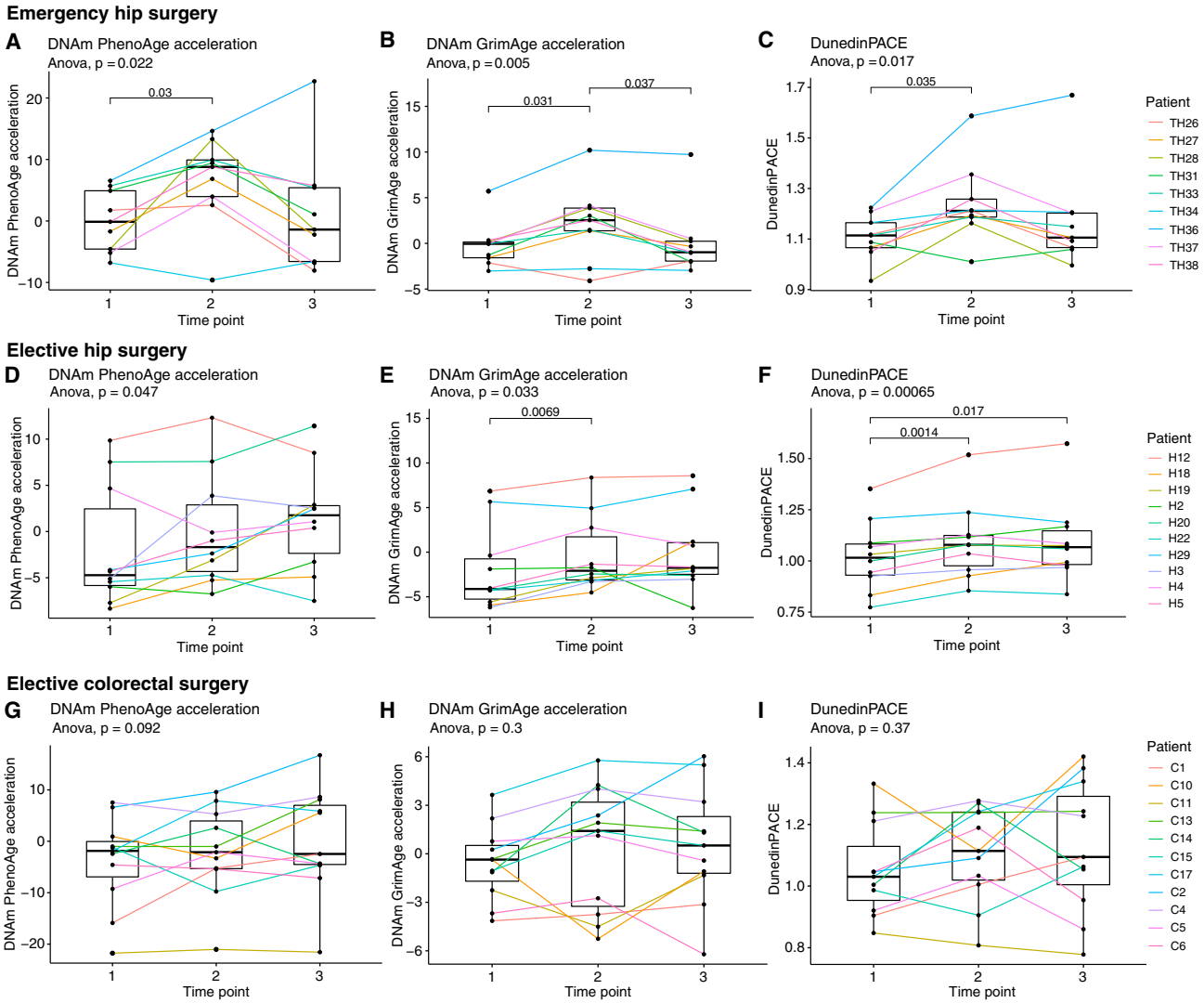

Figure 3. Patients undergoing major emergency (but not elective) surgery experience a reversible increase in biological age

(A–C) Second-generation DNAm age biomarkers for patients undergoing emergency surgery to repair traumatic hip fractures determined using DNAmPhenoAge (A), DNAmGrimAge (B), and DunedinPoAm38 (C).

(D–F) As above, but for patients undergoing elective hip surgery.

(G–I) As above, but for patients undergoing elective colorectal surgery.

In all panels, time point 1 corresponds to immediately before surgery; time point 2 corresponds to the morning after surgery; and time point 3 corresponds to the day of discharge from the hospital, 4–7 days post-surgery. p values were calculated with repeated-measures ANOVA and paired t tests. Sample sizes: (A–C), n = 9; (D–F), n = 10; (G–I), n = 11.

See also Figure S3.

In all three cohorts of surgical patients, first-generation DNAm clocks (Horvath DNAm age,[6] Hannum DNAm age,[7] and skin and blood DNAm age[8]) showed no significant changes (Figures S3A–S3C). A recent study introduced principal component (PC) corrected versions of the major human DNAm aging clocks to correct for technical noise and improve the performance of the clocks on longitudinal data.[28] The application of these PC clocks to our data yielded consistent results with the original versions of these clocks (Figures S3D–S3F). In some cases, first-generation PC clocks revealed significant changes that agreed with second-generation clocks; however, second-generation PC clocks still showed more consistent significant changes overall (we explore this further in other datasets below). Most importantly, the trends we observed using the original clocks agreed with those revealed by PC clocks: patients undergoing emergency hip surgery featured a reversible increase in biological age markers, patients undergoing elective hip surgery started at negative age accelerations and underwent a gradual increase toward baseline, and elective colorectal surgery had no effect on biological age markers.

We also utilized DNAm predictors of blood cell composition to analyze blood cell dynamics in this cohort of patients.[2,29] For patients undergoing emergency hip surgery, we found significant

Please cite this article in press as: Poganik et al., Biological age is increased by stress and restored upon recovery, Cell Metabolism (2023), https://doi.org/10.1016/j.cmet.2023.03.015

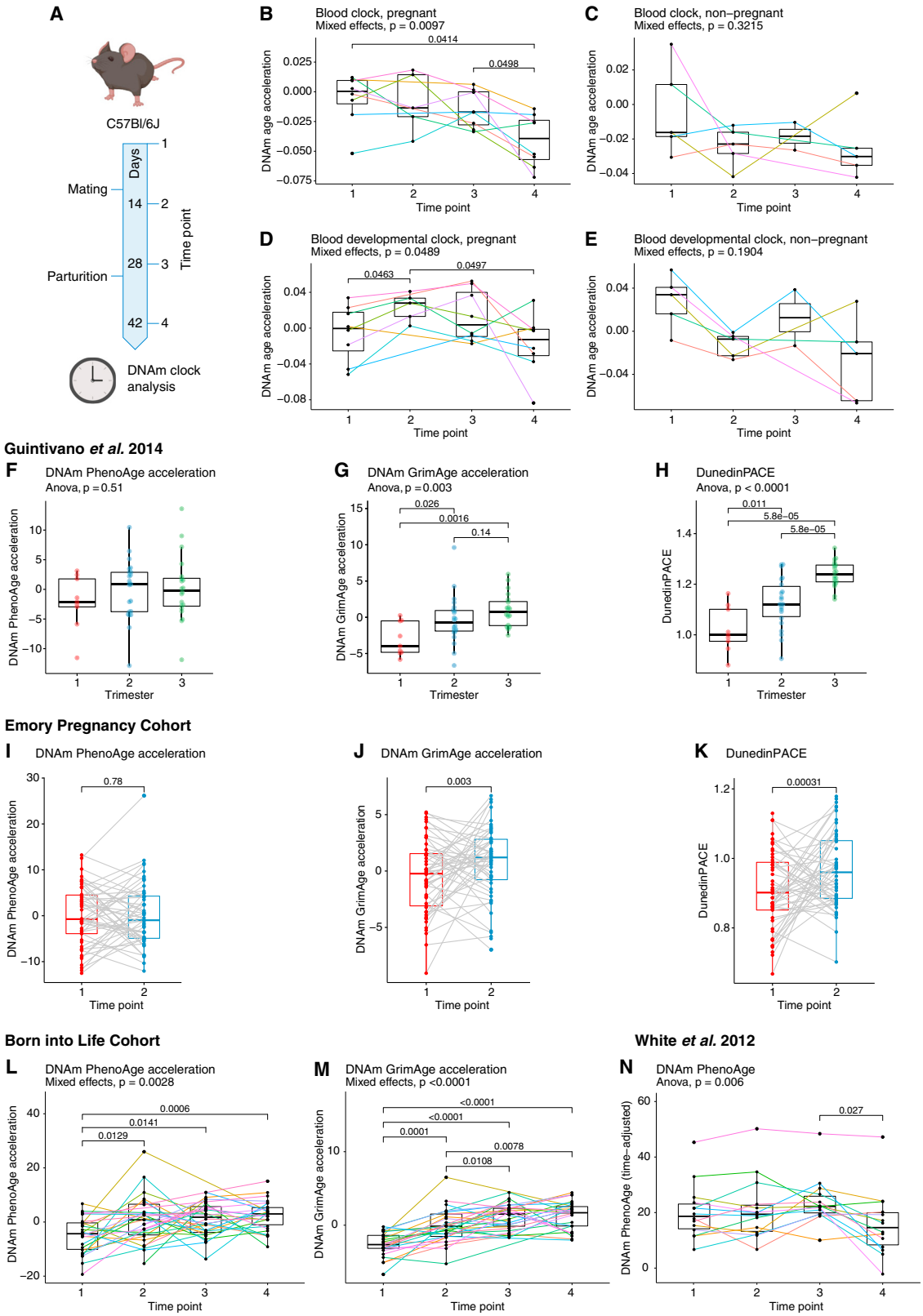

Figure 4. Mice and humans experience an increase in biological age over the course of pregnancy that is reversed following parturition

(A) Timeline of mouse pregnancy study. Note that "days" here refers to experimental days, not embryonic ages. Blood was collected from C57BL/6 mice before, during, and after pregnancy, and DNA isolated from this blood was subjected to DNAm clock analysis.

(legend continued on next page)

differences in the counts of B cells, several subsets of T cells, plasmablasts, natural killer (NK) cells, and monocytes. Patients undergoing elective hip surgery experienced significant fluctuation in levels of plasmablasts, NKs, and monocytes, and patients undergoing elective colorectal surgery showed no significant fluctuations in any of the cell types analyzed (Figures S3G–S3I).

Biological age of mice reversibly increases during pregnancy

We further examined reversible changes in biological age by testing the effect of pregnancy, given the significant biological overlap between pregnancy and aging. Pregnancy is a highly physiologically stressful event, with nearly every organ system subject to increased demand to support the developing fetus.[30] Because of the resulting damage accumulation and increased incidence of age-related diseases such as diabetes and heart disease, pregnancy has even been suggested as a model for aging.[31] With these considerations in mind, we hypothesized that biological age would increase over the course of pregnancy and return to baseline following delivery.

We began by studying a mouse model of pregnancy. Following a baseline blood sample, C57BL/6 mice were mated, and two blood samples were taken during the early and late phases of their pregnancies. Following parturition and a period of recovery, a final blood sample was collected (Figure 4A). We subjected DNA isolated from these blood samples to the HorvathMammalMethylChip40 for methylation profiling. The mouse blood clock revealed a significant decrease in biological age following parturition (Figure 4B), but no change in age-matched mice that were also mated but did not become pregnant (Figure 4C). Interestingly, the blood developmental clock showed an increase in biological age after mice became pregnant that resolved following parturition and recovery (Figure 4D). Again, no significant change was detected by this clock in non-pregnant animals (Figure 4E). We suspect that since the developmental clock was built using CpGs whose methylation levels change during development, this clock may be more suitable to evaluate pregnancy, a developmentally relevant process. In any event, taking the two clocks together, we conclude that pregnancy may induce a reversible increase in biological age.

Human pregnancy causes a reversible increase in biological age

To corroborate and expand on our results in mice, we analyzed methylation datasets from several cohorts of pregnant humans (Table S2). Most available longitudinal methylation datasets tracking women over the course of pregnancy cover the period from pre-/early pregnancy up to (or very shortly after) delivery. A cross-sectional dataset[33] of 54 pregnant American women from whom blood was sampled during one trimester of their pregnancy showed no difference in DNAmPhenoAge acceleration (Figure 4F), but a significant increase in biological age markers from the first to third trimesters was found using DNAmGrimAge (Figure 4G), and DunedinPACE revealed significant increases between both the first to second and second to third trimesters (Figure 4H). Similarly, DNAmGrimAge and DunedinPACE, but not DNAmPhenoAge, revealed an increase in biological age from early to late pregnancy in a longitudinal dataset[34] consisting of African American women who each provided two blood samples over the course of their pregnancies (Figures 4I–4K). In a cohort of pregnant Swedish women,[35,36] both DNAmPhenoAge and DNAmGrimAge revealed a progressive increase in biological age from pre-pregnancy (time point 1) to 2–4 days postpartum (time point 4) (Figures 4L and 4M). Thus, biological age increases in human pregnancy up to the point of parturition, consistent with the effects we found in mice. As with our human surgery data analysis (Figure S3), first-generation clocks did not detect any changes in these pregnancy datasets (Figures S4A–S4C). PC versions of first-generation clocks also did not detect significant changes in any of the datasets to which we were able to apply them (Figures S4E–S4G). PC versions of second-generation clocks yielded consistent results with original clocks (Figures S4E–S4G).

We identified one dataset[32] in which women were tracked longitudinally over the course of their pregnancy through 6 weeks postpartum. However, methylation profiling for this cohort was performed using the Illumina HumanMethylation27 beadchip, which limited the number of clocks we could apply to the Horvath multi-tissue clock and DNAmPhenoAge. DNAmPhenoAge (corrected for the passage of time, as chronological ages were not available for this dataset; see STAR Methods) revealed a trend toward higher biological age at delivery, followed by a significant

(B and C) Blood clock DNAm age acceleration results from pregnant (B) and non-pregnant (C) mice.
(D and E) Blood developmental clock DNAm age acceleration results from pregnant (D) and non-pregnant (E) mice.
(F–H) Cross-sectional DNAm age acceleration analysis of pregnant Americans across the three trimesters of pregnancy using DNAmPhenoAge (F), DNAmGrimAge (G), and DunedinPACE (H).
(I–K) DNAm age biomarkers (as in F–H) for a longitudinal study of pregnant African Americans with two blood samples collected over the course of pregnancy. Time point 1 corresponds to 7–15 weeks of pregnancy; time point 2 corresponds to 24–32 weeks of pregnancy.
(L and M) DNAmPhenoAge (L) and DNAmGrimAge (M) acceleration results from Swedish mothers longitudinally tracked over the course of pregnancy. Time point 1 corresponds to pre-pregnancy; time point 2 corresponds to 10–14 weeks of pregnancy; time point 3 corresponds to 26–28 weeks of pregnancy; time point 4 corresponds to 2–4 days postpartum.
(N) DNAmPhenoAge (adjusted for the passage of time; see STAR Methods for details) for a cohort of American mothers longitudinally tracked over the course of pregnancy and postpartum. Time point 1 corresponds to early pregnancy; time point 2 corresponds to mid-pregnancy; time point 3 corresponds to delivery; time point 4 corresponds to 6 weeks postpartum. p values were calculated using either repeated-measures ANOVA and paired t tests or a mixed effects model with post hoc pairwise comparison testing (see STAR Methods). Sample sizes: (B and D), n = 8 animals total from which up to 4 samples were collected; (C and E), n = 5 animals total from which up to 4 samples were collected; (F–H), n = 9, 22, and 20 for trimesters 1, 2, and 3, respectively; (I–K), n = 53; (L and M), n = 33 total subjects who each provided up to 4 samples; (N), n = 14. Note that for the Born into Life Cohort, due to data sharing limitations, we were unable to obtain the CpG data necessary to analyze DunedinPACE. Note also that the White et al.[32] dataset was generated using the Illumina HumanMethylation27 Beadchip, which limited our analysis to DNAm PhenoAge (N) and Horvath DNAm age (Figure S4D).
See also Figure S4.

Please cite this article in press as: Poganik et al., Biological age is increased by stress and restored upon recovery, Cell Metabolism (2023), https://doi.org/10.1016/j.cmet.2023.03.015

Table 1. Metadata and descriptive statistics of the COVID-19 patient cohort

	Female	Male	t test p value
n (%)	10 (34.5%)	19 (65.5%)	–
Mechanically ventilated (%)	10 (100%)	19 (100%)	–
Age (SD)	59.53 (20.27)	61.39 (12.54)	0.7616
Duration of hospitalization (SD)	30.9 (10.56)	43.68 (23.19)	0.1116
Duration of intensive care (SD)	15.7 (7.0)	21.47 (14.94)	0.2602

reversal of biological age markers at 6 weeks postpartum (Figure 4N), consistent with our mouse data above. Horvath DNAm age closely mirrored the overall trend but did not rise to the level of statistical significance (Figure S4D). Analyses of blood cell composition predicted from methylation data for the human pregnancy cohorts did not reveal consistent changes in cell composition over the course of pregnancy between datasets (Figures S4H–S4J). Thus, it is unlikely that changes in blood composition alone can explain the highly consistent effects we observe on biological age markers. Taking all our analyses in mice and humans together, we conclude that pregnancy induces a reversible increase in biological age markers, peaking around delivery and resolving postpartum.

Severe COVID-19 causes a reversible increase in biological age

We next hypothesized that severe infectious disease might cause reversible changes in biological age markers. COVID-19 is an ideal test case given its strong links to aging.[37,38] Not only are the elderly up to 90-fold more vulnerable to death from COVID-19,[39] but we and others have previously reported that accelerated biological age is associated with the incidence and severity of COVID-19.[40–44] Longitudinal biological age data covering the COVID-19 disease course is also extremely limited. A recent report included a subset of longitudinal samples, but the sample size (n = 3) precluded any statistical analysis.[44] We therefore sought to investigate whether COVID-19 induces a reversible change in biological age markers.

To directly test how biological age markers change over the course of severe infectious disease, we obtained longitudinal blood samples from patients with COVID-19. Our cohort consisted of patients who tested positive for COVID-19 by RT-PCR, were admitted to an intensive care unit, survived the disease, and provided multiple blood samples spanning the course of their hospitalization (Table 1). Because the patients in our cohort were generally already admitted to the ICU by the time the first available blood sample was taken, we hypothesized that the major effect we would observe was a reversal of *already* accelerated biological age markers. Given the known differences in both disease course and outcomes in males and females (with males generally experiencing poorer outcomes[45]), we separated our analysis by sex.

DNAmPhenoAge indicated a significant reversal of biological age in females following discharge from the ICU (i.e., time points 3–4), but no significant change in males (Figure 5A). Similarly, DNAmGrimAge indicated an increase in biological age that was partially reversed by the time of ICU discharge for females. This was marginally significant overall, and no significant change was observed in males (Figure 5B). In both cases, we note that male patients exhibited much more heterogeneity in the trajectories of their biological age markers over the disease course.

In the case of DunedinPACE (in which the normal pace of aging is 1), we found that the pace of aging was already elevated by ~25% by the point of ICU admission (time point 1) for both sexes. This was reversed following discharge from the ICU, although not fully to baseline (Figure 5C). As in all cases involving human samples above, first-generation clocks did not detect any changes in either males or females (Figures S5A and S5B). PC clock results generally did not rise to the level of statistical significance, although trends for second-generation PC clocks were consistent with the original second-generation clocks (Figures S5C and S5D). Few types of blood cells showed significant variation over the course of the disease, and those that did ($CD4^+$ T cells, plasmablasts, NKs, granulocytes) did not change consistently between male and female patients (Figures S5E and S5F). On the whole, we conclude that a severe infectious disease such as COVID-19 can induce a reversible increase in biological age, although the results are nuanced and seem to be both sex- and clock-specific.

Reversal of elevated biological age can be used to predict anti-aging interventions

The observed reversal in biological age markers of patients with COVID-19 following discharge from the ICU provides a tool with which to predict interventions that may potentially allow patients to recover their biological age more rapidly following a stressful event. We thus investigated the effect of experimental interventions received by our COVID-19 patient cohort on their ability to reverse their increased biological age. Largely due to the timeframe during which these samples were collected (March–June 2020), this group of interventions included hydroxychloroquine, remdesivir, and tocilizumab.[46] We calculated biological age recovery by subtracting biological age at time point 4 ($\geq$7 days after ICU discharge) from time point 3 (ICU discharge). Neither the anti-malarial hydroxychloroquine nor the broad-spectrum antiviral remdesivir showed any effects on biological age recovery (Figures 5D and 5E). Interestingly, however, patients treated with tocilizumab, a monoclonal antibody targeting the interleukin-6 receptor, showed a greater recovery of biological age (by all three second-generation clocks) than patients that did not receive this intervention (Figure 5F). Thus, tocilizumab may warrant further investigation as an anti-aging drug.

Common changes in DNAm across models of stress and recovery

We finally sought to understand whether changes in methylation induced by stress and/or recovery occurred at common CpG sites between the various models we examined. The intersection of significantly differentially methylated CpG sites across our human models revealed common sets of CpGs: 113 and 1,688 whose methylation increased and decreased, respectively, upon exposure to stress (Figures S6A and S6B; Table S3), and 80 and 3 whose methylation increased and decreased, respectively, upon recovery (Figures S6C and S6D; Table S3). We

Please cite this article in press as: Poganik et al., Biological age is increased by stress and restored upon recovery, Cell Metabolism (2023), https://doi.org/10.1016/j.cmet.2023.03.015

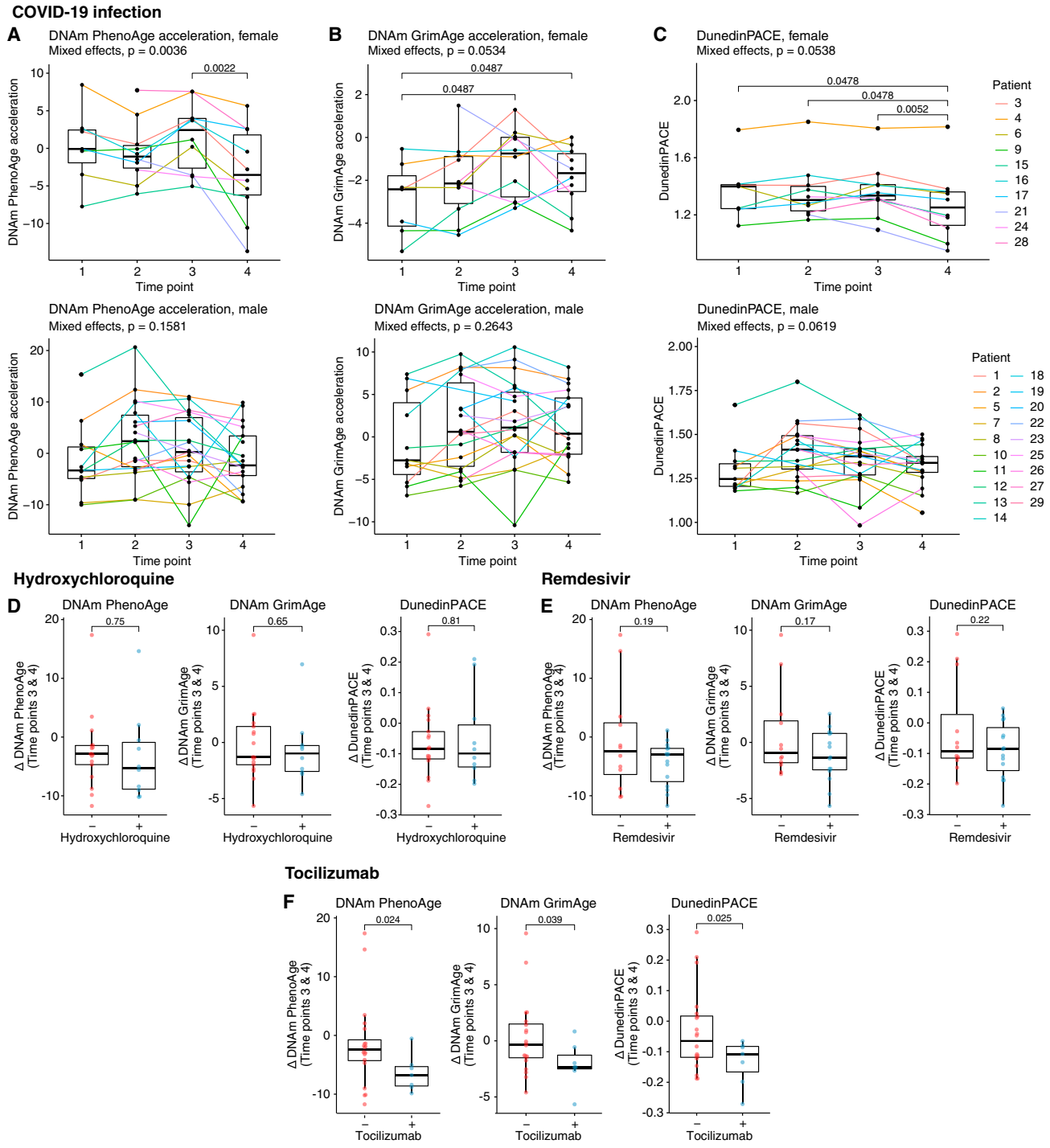

Figure 5. Patients with severe COVID-19 experience a reversible increase in DNAm age; treatment with tocilizumab enhances DNAm age recovery following ICU discharge

(A–C) DNAm age acceleration results for DNAmPhenoAge (A), DNAmGrimAge (B), and DunedinPACE (C). All upper panels show data for female patients and all lower panels show data for male patients. Time point 1 is within 5 days of ICU admission; time point 2 is within 5 days of the midpoint of the ICU stay; time point 3 is within 5 days of the date of discharge from the ICU; time point 4 is ≥7 days post-ICU discharge.

(D–F) DNAm age recovery, defined as the difference in DNAm age acceleration between time points 3 and 4), for patients treated with hydroxychloroquine (D), remdesivir (E), or tocilizumab (F). In (A)–(C), p values were calculated using a mixed effects model with post hoc pairwise comparison testing. In (D)–(F), p values were calculated with unpaired t tests. Sample sizes: (A–C), n = 10 female and n = 19 male subjects total who each provided up to 4 samples; (D), n = 19 untreated and 10 treated patients; (E), n = 12 untreated and 17 treated patients; (F), n = 21 untreated and 8 treated patients.

See also Figure S5.

Please cite this article in press as: Poganik et al., Biological age is increased by stress and restored upon recovery, Cell Metabolism (2023), https://doi.org/10.1016/j.cmet.2023.03.015

note that the analysis of recovery is inherently limited by the use of the HumanMethylation27 array for one of the recovery datasets, which only assays 27,000 CpGs. Nevertheless, these results demonstrate that a subset of CpGs may undergo common changes in methylation levels upon exposure to diverse forms of severe stress and upon recovery.

DISCUSSION

This study reveals that the biological age of humans and mice is not static nor steadily increasing but undergoes reversible changes over relatively short time periods of days to months according to multiple independent epigenetic aging clocks. This finding of fluid, fluctuating, malleable age challenges the long-standing conception of a unidirectional upward trajectory of biological age over the life course. Previous reports have hinted at the possibility of short-term fluctuations in biological age,[47–51] but the question of whether such changes are reversible has, until now, remained unexplored. Critically, the triggers of such changes were also unknown. We established that a reversible biological age change can be experimentally induced in animals subjected to heterochronic parabiosis. An increase in biological age upon exposure to aged blood is consistent with previous reports of detrimental age-related changes upon heterochronic blood exchange procedures.[52–54] However, the reversibility of such changes, as we observed (Figures 1, 2, and S1), has not yet been reported. From this initial insight, we hypothesized that other naturally occurring situations might also trigger reversible changes in biological age.

A clear pattern that emerged over the course of our studies is that exposure to stress increased biological age. When the stress was relieved, biological age could be fully or partially restored. This is perhaps most clearly demonstrated by our analysis of biological age changes in response to major surgery (Figure 3). Although we did not observe the effect in the case of elective surgeries, where patients are pre-screened for surgical candidacy and advised to follow strict preparation guidelines[27] (likely reflected in the lower biological age found in these patients on the day of their surgery), we saw a strong and rapid increase in biological age in trauma patients following emergency surgery. This is consistent with the higher risk of mortality and major postoperative complications associated with emergency hip repair.[55] Nevertheless, this increase was reversed and biological age was restored to baseline in the days following the surgery. Of note, the patients in this cohort were elderly (mean age 77.9 years), implying, surprisingly, that even people of advanced chronological age have the capacity to reverse a stress-induced increase in their biological age. Reversible changes in biological age were also found in response to pregnancy and COVID-19, implying that such changes may be rather common responses to stress. These situations (and others yet to be discovered) that trigger a rapid increase in biological age are likely good candidate models for testing the ability of anti-aging drugs to improve clinical outcomes. Moreover, our finding that biological age reversal is achievable on the scale of days (Figures 3A–3C, cf. time points 2–3) strongly points to the potential utility of anti-aging drugs in diseases/medical interventions that lead to increased stress, such as major surgery. The ability of tocilizumab to enhance the biological age recovery of convalescent COVID-19 patients (Figure 5F) lends further credence to this notion.

From a technical standpoint, across human datasets examined, we consistently observed that first-generation DNAm clocks were not able to detect significant effects found by second-generation clocks applied to the same data, even after PC correction in nearly all cases.[28] Interestingly, a recent study examining the effects of adolescent habits on biological aging reported a similar observation on first- vs. second-generation clocks,[56] as have other recent studies.[57] This may imply that the integration of multiple age-related biomarkers into the models of second-generation clocks renders them more sensitive to transient fluctuations in biological age compared with first-generation clocks, which are trained only on chronological age. On the other hand, we were able to observe fluctuations in the biological age of pregnant mice using first-generation mouse clocks, though we suspect that this is because inbred mice simply represent a biologically simpler system overall and far more mouse data is available with which to train first-generation clocks. Whatever the underlying reason, these data highlight the critical importance of the judicious selection of DNAm clocks appropriate to the analysis at hand, especially in light of the many clocks continuously coming to the fore. Nevertheless, we obtained consistent outputs across second-generation clocks applied across our human DNAm datasets, as well as the agreement with mouse models in the case of pregnancy, bolstering our confidence in our conclusions.

In the most fundamental sense, our data reveal the dynamic nature of biological age: stress can trigger a rapid increase in biological age, which can be reversed. Importantly, this implies both the existence of intrinsic mechanisms to reverse increased biological age and the opportunity to reverse transient increases in biological age therapeutically. The findings also imply that severe stress increases mortality, at least in part, by increasing biological age. This notion immediately suggests that mortality may be decreased by reducing biological age and that the ability to recover from stress may be an important determinant of successful aging and longevity. Finally, biological age may be a useful parameter in assessing physiological stress and its relief.

Limitations of the study

Although this study highlights a previously unappreciated aspect of the nature of biological aging, we acknowledge some important limitations. First, although we characterized our parabiosis model at multiple omics levels, we relied mainly on DNAm clocks to infer biological age in our human studies. This is because these tools are the most powerful aging biomarker currently available. It is our hope that as the ongoing expansion of the aging biomarkers field proceeds, additional biomarkers that rival or exceed the power of DNAm clocks will allow us to confirm our conclusions using orthogonal approaches to measure biological age. Indeed, recent analyses of complete blood counts and physical activity are consistent with our findings of fluctuations in biological age across the entire life.[49,50]

Second, a critically important concern common to all studies that utilize biomarkers of aging is the discrimination of *bona fide* effects on biological aging from artifacts of the biomarkers. By artifacts, we mean changes in biomarker predictions driven

by something other than a *true* change in biological age, such as an as-yet-identified component of the immune response. Although no biomarker is perfect, several lines of evidence give us confidence that our observations represent true modulations of biological age: (1) DNAm age data in our parabiosis model was highly consistent with analyses at the transcriptomic and metabolomic levels; (2) where we were able to analyze across species, the effects were consistent; (3) we observed effects consistently with one class of DNAm biomarkers (second-generation clocks), but not another (first-generation clocks). We would expect artifactual "positive" results to occur randomly across the biomarkers analyzed. Furthermore, diverse algorithms within the second-generation clock class converge on the same results; and (4) several distinct models—surgery, pregnancy, and COVID-19—united by the severe physiological stress they induce, caused similar effects on the biomarkers. Future work will be needed to link, for instance, successful recovery of biological age following a stressful event to improved clinical outcome.

Finally, our findings are limited in their ability to probe the connections between short-term fluctuations in biological age and lifelong biological aging trajectories. For instance, we observed the postpartum recovery of biological age in pregnant subjects. However, not all subjects seem to recover their biological age at the same rate or to the same extent. Future work may focus on, for example, the association of postpartum complications with the rate/degree of biological age recovery following pregnancy. Additionally, other reports indicate that increasing parity (i.e., number of pregnancies) is associated with accelerated DNAm age.[58,59] A key area for future study is understanding how transient elevations in biological age and/or successful recovery from such increases may contribute to accelerated aging over the life course.

STAR★METHODS

Detailed methods are provided in the online version of this paper and include the following:

- KEY RESOURCES TABLE
- RESOURCE AVAILABILITY
  - Lead contact
  - Materials availability
  - Data and code availability
- EXPERIMENTAL MODEL AND SUBJECT DETAILS
  - Mouse experiments
  - Mouse parabiosis experiments
  - Mouse pregnancy experiments
  - COVID-19 study
- METHOD DETAILS
  - Isolation of nucleic acids
  - DNA methylation profiling
  - Other sources of human methylation data
  - Gene expression profiling
  - Metabolite profiling
- QUANTIFICATION AND STATISTICAL ANALYSIS
  - DNAm clock analysis
  - DNAm age analysis
  - Gene expression analysis
  - Association with gene expression signatures
  - Functional enrichment analysis
  - Metabolomics analysis
  - Differential methylation analysis
  - Statistics

SUPPLEMENTAL INFORMATION

Supplemental information can be found online at https://doi.org/10.1016/j.cmet.2023.03.015.

ACKNOWLEDGMENTS

We thank Dr. Anastasia Shindyapina (Gladyshev Lab) and Nate Rogers (Brigham and Women's Hospital Center for Comparative Medicine) for training in mouse handling and blood collection. We thank Bobby Brooke of the Epigenetic Clock Development Foundation for the coordination of DNAm profiling. We thank Lindsay Rutte, Tim Janicki, and Dr. Lynn Bry of the Brigham and Women's Hospital Crimson Core Facility for assistance with COVID-19 sample acquisition. We thank Drs. Albert Higgins-Chen and Morgan E. Levine for sharing the PC clocks code prior to its publication. This study was funded by NIA grants (to V.N.G. and J.P.W. [R21AG065943]). J.R.P. is supported by the BWH Organ Design and Engineering Training Program, NIBIB grant 5T32EB016652-07. C.K. was supported by the European Union project RRF-2.3.1-21-2022-00004 within the framework of the Artificial Intelligence National Laboratory, Hungary.

AUTHOR CONTRIBUTIONS

Conceptualization, J.R.P. and V.N.G.; methodology, J.R.P., B.Z., A.T., A.D., C.K., S.H.Y., A.T.L., A.H., C.B.C., S.H., J.P.W., and V.N.G.; investigation, J.R.P., B.Z., A.T., A.D., C.K., A.T.L., A.H., and S.H.; essential data contribution, T.G., A.M.H., E.A., G.P., and C.A.; visualization, J.R.P.; funding acquisition, J.P.W. and V.N.G.; project administration, S.H., J.P.W., and V.N.G.; supervision, C.B.C., S.H., J.P.W., and V.N.G.; writing – original draft, J.R.P. and V.N.G.; writing – review & editing, J.R.P., B.Z., G.S.B., A.T., A.D., C.K., S.H.Y., A.T.L., A.H., T.G., A.M.H., E.A., G.P., C.A., C.B.C., S.H., J.P.W., and V.N.G.

DECLARATION OF INTERESTS

The authors declare no competing interests.

INCLUSION AND DIVERSITY

We support inclusive, diverse, and equitable conduct of research.

Received: June 7, 2022
Revised: December 22, 2022
Accepted: March 20, 2023
Published: April 21, 2023

REFERENCES

1. Zhang, B., and Gladyshev, V.N. (2020). How can aging be reversed? Exploring rejuvenation from a damage-based perspective. Adv. Genet. (Hoboken) *1*, e10025. https://doi.org/10.1002/ggn2.10025.
2. Horvath, S., and Levine, A.J. (2015). HIV-1 infection accelerates age according to the epigenetic clock. J. Infect. Dis. *212*, 1563–1573. https://doi.org/10.1093/infdis/jiv277.
3. Wang, T., Tsui, B., Kreisberg, J.F., Robertson, N.A., Gross, A.M., Yu, M.K., Carter, H., Brown-Borg, H.M., Adams, P.D., and Ideker, T. (2017). Epigenetic aging signatures in mice livers are slowed by dwarfism, calorie restriction and rapamycin treatment. Genome Biol. *18*, 57. https://doi.org/10.1186/s13059-017-1186-2.
4. Quach, A., Levine, M.E., Tanaka, T., Lu, A.T., Chen, B.H., Ferrucci, L., Ritz, B., Bandinelli, S., Neuhouser, M.L., Beasley, J.M., et al. (2017). Epigenetic

clock analysis of diet, exercise, education, and lifestyle factors. Aging *9*, 419–446. https://doi.org/10.18632/aging.101168.

5. Nwanaji-Enwerem, J.C., Colicino, E., Trevisi, L., Kloog, I., Just, A.C., Shen, J., Brennan, K., Dereix, A., Hou, L., Vokonas, P., et al. (2016). Long-term ambient particle exposures and blood DNA methylation age: findings from the VA normative aging study. Environ. Epigenet. *2*, 74510–74525. https://doi.org/10.1093/eep/dvw006.
6. Horvath, S. (2013). DNA methylation age of human tissues and cell types. Genome Biol. *14*, R115. https://doi.org/10.1186/gb-2013-14-10-r115.
7. Hannum, G., Guinney, J., Zhao, L., Zhang, L., Hughes, G., Sadda, S., Klotzle, B., Bibikova, M., Fan, J.B., Gao, Y., et al. (2013). Genome-wide methylation profiles reveal quantitative views of human aging rates. Mol. Cell *49*, 359–367. https://doi.org/10.1016/j.molcel.2012.10.016.
8. Horvath, S., Oshima, J., Martin, G.M., Lu, A.T., Quach, A., Cohen, H., Felton, S., Matsuyama, M., Lowe, D., Kabacik, S., et al. (2018). Epigenetic clock for skin and blood cells applied to Hutchinson Gilford progeria Syndrome and ex vivo studies. Aging *10*, 1758–1775. https://doi.org/10.18632/aging.101508.
9. Mozhui, K., Lu, A., Li, C.Z., Haghani, A., Sandoval-Sierra, J.V., Williams, R.W., and Horvath, S. (2021). Genetic analyses of epigenetic predictors that estimate aging, metabolic traits, and lifespan. https://doi.org/10.1101/2021.06.23.449634v2.
10. Meer, M.V., Podolskiy, D.I., Tyshkovskiy, A., and Gladyshev, V.N. (2018). A whole lifespan mouse multi-tissue DNA methylation clock. eLife *7*, e40675. https://doi.org/10.7554/eLife.40675.
11. Petkovich, D.A., Podolskiy, D.I., Lobanov, A.V., Lee, S.G., Miller, R.A., and Gladyshev, V.N. (2017). Using DNA methylation profiling to evaluate biological age and longevity interventions. Cell Metab. *25*, 954–960.e6. https://doi.org/10.1016/j.cmet.2017.03.016.
12. Stubbs, T.M., Bonder, M.J., Stark, A.K., Krueger, F., BI Ageing Clock Team, von Meyenn, F., Stegle, O., and Reik, W. (2017). Multi-tissue DNA methylation age predictor in mouse. Genome Biol. *18*, 68. https://doi.org/10.1186/s13059-017-1203-5.
13. Thompson, M.J., Chwiałkowska, K., Rubbi, L., Lusis, A.J., Davis, R.C., Srivastava, A., Korstanje, R., Churchill, G.A., Horvath, S., and Pellegrini, M. (2018). A multi-tissue full lifespan epigenetic clock for mice. Aging *10*, 2832–2854. https://doi.org/10.18632/aging.101590.
14. Levine, M.E., Lu, A.T., Quach, A., Chen, B.H., Assimes, T.L., Bandinelli, S., Hou, L., Baccarelli, A.A., Stewart, J.D., Li, Y., et al. (2018). An epigenetic biomarker of aging for lifespan and healthspan. Aging *10*, 573–591. https://doi.org/10.18632/aging.101414.
15. Lu, A.T., Quach, A., Wilson, J.G., Reiner, A.P., Aviv, A., Raj, K., Hou, L., Baccarelli, A.A., Li, Y., Stewart, J.D., et al. (2019). DNA methylation GrimAge strongly predicts lifespan and healthspan. Aging *11*, 303–327. https://doi.org/10.18632/aging.101684.
16. Belsky, D.W., Caspi, A., Arseneault, L., Baccarelli, A., Corcoran, D.L., Gao, X., Hannon, E., Harrington, H.L., Rasmussen, L.J., Houts, R., et al. (2020). Quantification of the pace of biological aging in humans through a blood test, the DunedinPoAm DNA methylation algorithm. eLife *9*, e54870. https://doi.org/10.7554/eLife.54870.
17. Belsky, D.W., Caspi, A., Corcoran, D.L., Sugden, K., Poulton, R., Arseneault, L., Baccarelli, A., Chamarti, K., Gao, X., Hannon, E., et al. (2022). DunedinPACE, a DNA methylation biomarker of the pace of aging. eLife *11*, e73420. https://doi.org/10.7554/eLife.73420.
18. Fahy, G.M., Brooke, R.T., Watson, J.P., Good, Z., Vasanawala, S.S., Maecker, H., Leipold, M.D., Lin, D.T.S., Kobor, M.S., and Horvath, S. (2019). Reversal of epigenetic aging and immunosenescent trends in humans. Aging Cell *18*, e13028. https://doi.org/10.1111/acel.13028.
19. Conboy, I.M., and Rando, T.A. (2012). Heterochronic parabiosis for the study of the effects of aging on stem cells and their niches. Cell Cycle *11*, 2260–2267. https://doi.org/10.4161/cc.20437.
20. Zhang, B., Lee, D.E., Trapp, A., Tyshkovskiy, A., Lu, A.T., Bareja, A., Kerepesi, C., Katz, L.H., Shindyapina, A.V., Dmitriev, S.E., et al. (2021). Multi-omic rejuvenation and lifespan extension upon exposure to youthful circulation. Preprint at bioRxiv. https://doi.org/10.1101/2021.11.11.468258.
21. Arneson, A., Haghani, A., Thompson, M.J., Pellegrini, M., Kwon, S.B., Vu, H., Maciejewski, E., Yao, M., Li, C.Z., Lu, A.T., et al. (2022). A mammalian methylation array for profiling methylation levels at conserved sequences. Nat. Commun. *13*, 783. https://doi.org/10.1038/s41467-022-28355-z.
22. Mammalian; Methylation Consortium, Lu, A.T., Fei, Z., Haghani, A., Robeck, T.R., Zoller, J.A., Li, C.Z., Zhang, J., Ablaeva, J., Adams, D.M., et al. (2021). Universal DNA methylation age across mammalian tissues. https://doi.org/10.1101/2021.01.18.426733.
23. Tyshkovskiy, A., Bozaykut, P., Borodinova, A.A., Gerashchenko, M.V., Ables, G.P., Garratt, M., Khaitovich, P., Clish, C.B., Miller, R.A., and Gladyshev, V.N. (2019). Identification and application of gene expression signatures associated with lifespan extension. Cell Metab. *30*, 573–593.e8. https://doi.org/10.1016/j.cmet.2019.06.018.
24. Wolf, E.J., Maniates, H., Nugent, N., Maihofer, A.X., Armstrong, D., Ratanatharathorn, A., Ashley-Koch, A.E., Garrett, M., Kimbrel, N.A., Lori, A., et al. (2018). Traumatic stress and accelerated DNA methylation age: A meta-analysis. Psychoneuroendocrinology *92*, 123–134. https://doi.org/10.1016/j.psyneuen.2017.12.007.
25. Zannas, A.S., Arloth, J., Carrillo-Roa, T., Iurato, S., Röh, S., Ressler, K.J., Nemeroff, C.B., Smith, A.K., Bradley, B., Heim, C., et al. (2015). Lifetime stress accelerates epigenetic aging in an urban, African American cohort: relevance of glucocorticoid signaling. Genome Biol. *16*, 266. https://doi.org/10.1186/s13059-015-0828-5.
26. Sadahiro, R., Knight, B., James, F., Hannon, E., Charity, J., Daniels, I.R., Burrage, J., Knox, O., Crawford, B., Smart, N.J., et al. (2020). Major surgery induces acute changes in measured DNA methylation associated with immune response pathways. Sci. Rep. *10*, 5743. https://doi.org/10.1038/s41598-020-62262-x.
27. Levett, D.Z.H., Edwards, M., Grocott, M., and Mythen, M. (2016). Preparing the patient for surgery to improve outcomes. Best Pract. Res. Clin. Anaesthesiol. *30*, 145–157. https://doi.org/10.1016/j.bpa.2016.04.002.
28. Higgins-Chen, A.T., Thrush, K.L., Wang, Y., Minteer, C.J., Kuo, P.L., Wang, M., Niimi, P., Sturm, G., Lin, J., Moore, A.Z., et al. (2022). A computational solution for bolstering reliability of epigenetic clocks: implications for clinical trials and longitudinal tracking. Nat. Aging *2*, 644–661. https://doi.org/10.1038/s43587-022-00248-2.
29. Houseman, E.A., Accomando, W.P., Koestler, D.C., Christensen, B.C., Marsit, C.J., Nelson, H.H., Wiencke, J.K., and Kelsey, K.T. (2012). DNA methylation arrays as surrogate measures of cell mixture distribution. BMC Bioinformatics *13*, 86. https://doi.org/10.1186/1471-2105-13-86.
30. Hill, C.C., and Pickinpaugh, J. (2008). Physiologic changes in pregnancy. Surg. Clin. North Am. *88*, 391–401. https://doi.org/10.1016/j.suc.2007.12.005.
31. Giller, A., Andrawus, M., Gutman, D., and Atzmon, G. (2020). Pregnancy as a model for aging. Ageing Res. Rev. *62*, 101093. https://doi.org/10.1016/j.arr.2020.101093.
32. White, W.M., Brost, B.C., Sun, Z., Rose, C., Craici, I., Wagner, S.J., Turner, S., and Garovic, V.D. (2012). Normal early pregnancy: a transient state of epigenetic change favoring hypomethylation. Epigenetics *7*, 729–734. https://doi.org/10.4161/epi.20388.
33. Guintivano, J., Arad, M., Gould, T.D., Payne, J.L., and Kaminsky, Z.A. (2014). Antenatal prediction of postpartum depression with blood DNA methylation biomarkers. Mol. Psychiatry *19*, 560–567. https://doi.org/10.1038/mp.2013.62.
34. Knight, A.K., Conneely, K.N., Kilaru, V., Cobb, D., Payne, J.L., Meilman, S., Corwin, E.J., Kaminsky, Z.A., Dunlop, A.L., and Smith, A.K. (2018). SLC9B1 methylation predicts fetal intolerance of labor. Epigenetics *13*, 33–39. https://doi.org/10.1080/15592294.2017.1411444.
35. Gruzieva, O., Merid, S.K., Chen, S., Mukherjee, N., Hedman, A.M., Almqvist, C., Andolf, E., Jiang, Y., Kere, J., Scheynius, A., et al. (2019).

DNA methylation trajectories during pregnancy. Epigenet. Insights *12*, 2516865719867090. https://doi.org/10.1177/2516865719867090.

36. Smew, A.I., Hedman, A.M., Chiesa, F., Ullemar, V., Andolf, E., Pershagen, G., and Almqvist, C. (2018). Limited association between markers of stress during pregnancy and fetal growth in 'Born into Life', a new prospective birth cohort. Acta Paediatr. *107*, 1003–1010. https://doi.org/10.1111/apa.14246.

37. Mavrikaki, M., Lee, J.D., Solomon, I.H., and Slack, F.J. (2022). Severe COVID-19 is associated with molecular signatures of aging in the human brain. Nat. Aging *2*, 1130–1137. https://doi.org/10.1038/s43587-022-00321-w.

38. Santesmasses, D., Castro, J.P., Zenin, A.A., Shindyapina, A.V., Gerashchenko, M.V., Zhang, B., Kerepesi, C., Yim, S.H., Fedichev, P.O., and Gladyshev, V.N. (2020). COVID-19 is an emergent disease of aging. Aging Cell *19*, e13230. https://doi.org/10.1111/acel.13230.

39. CDC (2020). Cases, data, and surveillance. Cent. Dis. control prev. https://www.cdc.gov/coronavirus/2019-ncov/covid-data/investigations-discovery/hospitalization-death-by-age.html.

40. Ying, K., Zhai, R., Pyrkov, T.V., Shindyapina, A.V., Mariotti, M., Fedichev, P.O., Shen, X., and Gladyshev, V.N. (2021). Genetic and phenotypic analysis of the causal relationship between aging and COVID-19. Commun. Med. (Lond) *1*, 35. https://doi.org/10.1038/s43856-021-00033-z.

41. Kuo, C.L., Pilling, L.C., Atkins, J.L., Masoli, J.A.H., Delgado, J., Tignanelli, C., Kuchel, G.A., Melzer, D., Beckman, K.B., and Levine, M.E. (2021). Biological aging predicts vulnerability to COVID-19 severity in UK Biobank participants. J. Gerontol. A Biol. Sci. Med. Sci. *76*, e133–e141. https://doi.org/10.1093/gerona/glab060.

42. Franzen, J., Nüchtern, S., Tharmapalan, V., Vieri, M., Nikolić, M., Han, Y., Balfanz, P., Marx, N., Dreher, M., Brümmendorf, T.H., et al. (2020). Epigenetic clocks are not accelerated in COVID-19 patients. IJMS *22*, 9306. https://doi.org/10.3390/ijms22179306.

43. Pang, A.P., Higgins-Chen, A.T., Comite, F., Raica, I., Arboleda, C., Mendez, T., Schotsaert, M., Dwaraka, V., Smith, R., Levine, M.E., et al. (2021). Longitudinal study of DNA methylation and epigenetic clocks prior to and following test-confirmed COVID-19 and mRNA vaccination (infectious diseases (except HIV/AIDS)). https://doi.org/10.1101/2021.12.01.21266670.

44. Cao, X., Li, W., Wang, T., Ran, D., Davalos, V., Planas-Serra, L., Pujol, A., Esteller, M., Wang, X., and Yu, H. (2022). Accelerated biological aging in COVID-19 patients. Nat. Commun. *13*, 2135. https://doi.org/10.1038/s41467-022-29801-8.

45. Peckham, H., de Gruijter, N.M., Raine, C., Radziszewska, A., Ciurtin, C., Wedderburn, L.R., Rosser, E.C., Webb, K., and Deakin, C.T. (2020). Male sex identified by global COVID-19 meta-analysis as a risk factor for death and ITU admission. Nat. Commun. *11*, 6317. https://doi.org/10.1038/s41467-020-19741-6.

46. Sanders, J.M., Monogue, M.L., Jodlowski, T.Z., and Cutrell, J.B. (2020). Pharmacologic treatments for coronavirus disease 2019 (COVID-19): a review. JAMA *323*, 1824–1836. https://doi.org/10.1001/jama.2020.6019.

47. Chen, R., Xia, L., Tu, K., Duan, M., Kukurba, K., Li-Pook-Than, J., Xie, D., and Snyder, M. (2018). Longitudinal personal DNA methylome dynamics in a human with a chronic condition. Nat. Med. *24*, 1930–1939. https://doi.org/10.1038/s41591-018-0237-x.

48. Lu, Y., Brommer, B., Tian, X., Krishnan, A., Meer, M., Wang, C., Vera, D.L., Zeng, Q., Yu, D., Bonkowski, M.S., et al. (2020). Reprogramming to recover youthful epigenetic information and restore vision. Nature *588*, 124–129. https://doi.org/10.1038/s41586-020-2975-4.

49. Pyrkov, T.V., Avchaciov, K., Tarkhov, A.E., Menshikov, L.I., Gudkov, A.V., and Fedichev, P.O. (2021). Longitudinal analysis of blood markers reveals progressive loss of resilience and predicts human lifespan limit. Nat. Commun. *12*, 2765. https://doi.org/10.1038/s41467-021-23014-1.

50. Avchaciov, K., Antoch, M.P., Andrianova, E.L., Tarkhov, A.E., Menshikov, L.I., Burmistrova, O., Gudkov, A.V., and Fedichev, P.O. (2022). Unsupervised learning of aging principles from longitudinal data. Nat. Commun. *13*, 6529. https://doi.org/10.1038/s41467-022-34051-9.

51. Komaki, S., Ohmomo, H., Hachiya, T., Sutoh, Y., Ono, K., Furukawa, R., Umekage, S., Otsuka-Yamasaki, Y., Minabe, S., Takashima, A., et al. (2022). Evaluation of short-term epigenetic age fluctuation. Clin. Epigenet. *14*, 76. https://doi.org/10.1186/s13148-022-01293-9.

52. Rebo, J., Mehdipour, M., Gathwala, R., Causey, K., Liu, Y., Conboy, M.J., and Conboy, I.M. (2016). A single heterochronic blood exchange reveals rapid inhibition of multiple tissues by old blood. Nat. Commun. *7*, 13363. https://doi.org/10.1038/ncomms13363.

53. Gonzalez-Armenta, J.L., Li, N., Lee, R.L., Lu, B., and Molina, A.J.A. (2021). Heterochronic parabiosis: old blood induces changes in mitochondrial structure and function of young mice. J. Gerontol. A Biol. Sci. Med. Sci. *76*, 434–439. https://doi.org/10.1093/gerona/glaa299.

54. Kiss, T., Nyúl-Tóth, Á., Gulej, R., Tarantini, S., Csipo, T., Mukli, P., Ungvari, A., Balasubramanian, P., Yabluchanskiy, A., Benyo, Z., et al. (2022). Old blood from heterochronic parabionts accelerates vascular aging in young mice: transcriptomic signature of pathologic smooth muscle remodeling. GeroScience *44*, 953–981. https://doi.org/10.1007/s11357-022-00519-1.

55. Le Manach, Y., Collins, G., Bhandari, M., Bessissow, A., Boddaert, J., Khiami, F., Chaudhry, H., De Beer, J., Riou, B., Landais, P., et al. (2015). Outcomes after hip fracture surgery compared with elective total hip replacement. JAMA *314*, 1159–1166. https://doi.org/10.1001/jama.2015.10842.

56. Kankaanpää, A., Tolvanen, A., Heikkinen, A., Kaprio, J., Ollikainen, M., and Sillanpää, E. (2022). The role of adolescent lifestyle habits in biological aging: A prospective twin study. eLife *11*, e80729. https://doi.org/10.7554/eLife.80729.

57. Raffington, L., and Belsky, D.W. (2022). Integrating DNA methylation measures of biological aging into social determinants of Health Research. Curr. Environ. Health Rep. *9*, 196–210. https://doi.org/10.1007/s40572-022-00338-8.

58. Ryan, C.P., Hayes, M.G., Lee, N.R., McDade, T.W., Jones, M.J., Kobor, M.S., Kuzawa, C.W., and Eisenberg, D.T.A. (2018). Reproduction predicts shorter telomeres and epigenetic age acceleration among young adult women. Sci. Rep. *8*, 11100. https://doi.org/10.1038/s41598-018-29486-4.

59. Kresovich, J.K., Harmon, Q.E., Xu, Z., Nichols, H.B., Sandler, D.P., and Taylor, J.A. (2019). Reproduction, DNA methylation and biological age. Hum. Reprod. *34*, 1965–1973. https://doi.org/10.1093/humrep/dez149.

60. Whitten, W.K. (1956). Modification of the oestrous cycle of the mouse by external stimuli associated with the male. J. Endocrinol. *13*, 399–404. https://doi.org/10.1677/joe.0.0130399.

61. Paynter, N.P., Balasubramanian, R., Giulianini, F., Wang, D.D., Tinker, L.F., Gopal, S., Deik, A.A., Bullock, K., Pierce, K.A., Scott, J., et al. (2018). Metabolic predictors of incident coronary heart disease in women. Circulation *137*, 841–853. https://doi.org/10.1161/CIRCULATIONAHA.117.029468.

62. Aryee, M.J., Jaffe, A.E., Corrada-Bravo, H., Ladd-Acosta, C., Feinberg, A.P., Hansen, K.D., and Irizarry, R.A. (2014). Minfi: a flexible and comprehensive Bioconductor package for the analysis of Infinium DNA methylation microarrays. Bioinformatics *30*, 1363–1369. https://doi.org/10.1093/bioinformatics/btu049.

63. Danbelsky. Dunedin PACE. 2022. https://github.com/danbelsky/DunedinPACE.

64. Anders, S., and Huber, W. (2010). Differential expression analysis for sequence count data. Genome Biol. *11*, R106. https://doi.org/10.1186/gb-2010-11-10-r106.

65. Robinson, M.D., McCarthy, D.J., and Smyth, G.K. (2010). edgeR: a Bioconductor package for differential expression analysis of digital gene expression data. Bioinformatics *26*, 139–140. https://doi.org/10.1093/bioinformatics/btp616.

66. Benjamini, Y., and Hochberg, Y. (1995). Controlling the false discovery rate: A practical and powerful approach to multiple testing. J. R. Stat. Soc. B *57*, 289–300. https://doi.org/10.1111/j.2517-6161.1995.tb02031.x.

67. Subramanian, A., Tamayo, P., Mootha, V.K., Mukherjee, S., Ebert, B.L., Gillette, M.A., Paulovich, A., Pomeroy, S.L., Golub, T.R., Lander, E.S.,

et al. (2005). Gene set enrichment analysis: A knowledge-based approach for interpreting genome-wide expression profiles. Proc. Natl. Acad. Sci. USA *102*, 15545–15550. https://doi.org/10.1073/pnas.0506580102.

68. Pang, Z., Chong, J., Zhou, G., de Lima Morais, D.A., Chang, L., Barrette, M., Gauthier, C., Jacques, P.É., Li, S., and Xia, J. (2021). MetaboAnalyst 5.0: narrowing the gap between raw spectra and functional insights. Nucleic Acids Res. *49*, W388–W396. https://doi.org/10.1093/nar/gkab382.

69. Zhou, W., Triche, T.J., Laird, P.W., and Shen, H. (2018). SeSAMe: reducing artifactual detection of DNA methylation by Infinium BeadChips in genomic deletions. Nucleic Acids Res. *46*, e123. https://doi.org/10.1093/nar/gky691.

Please cite this article in press as: Poganik et al., Biological age is increased by stress and restored upon recovery, Cell Metabolism (2023), https://doi.org/10.1016/j.cmet.2023.03.015

STAR★METHODS

KEY RESOURCES TABLE

REAGENT or RESOURCE	SOURCE	IDENTIFIER
Biological samples		
DNA isolated from blood of COVID-19 patients	Brigham and Women's Hospital Crimson Core	N/A
Critical commercial assays		
Infinium MethylationEPIC v2.0 Kit	Illumina	20087709
DNeasy Blood & Tissue Kit	Qiagen	69504
QIAamp DNA Blood Mini Kit	Qiagen	51104
RNAqueous Total RNA Isolation Kit	Invitrogen	AM1912
Deposited data		
Sadahiro et al.[26] DNAm data	GEO	GSE142536
Guintivano et al.[33] DNAm data	GEO	GSE44132
Emory Pregnancy Cohort DNAm data	GEO	GSE107459
Born into Life Cohort DNAm data	Prof. C. Almqvist	N/A
White et al.[32] DNAm data	GEO	GSE37722
Parabiosis data: HorvathMammalMethyl40 array DNAm, RRBS DNAm, and RNA-seq data	This study	GSE224447
Longitudinal mouse pregnancy DNAm data	This study	GSE224352
Longitudinal DNAm data for patients with severe COVID-19	This study	GSE226206
Experimental models: Organisms/strains		
C57Bl/6J mice	Jackson Laboratory	000664
Software and algorithms		
Prism	Graphpad	v9
R	r-project.org	v4.1.1
RStudio	Rstudio.com	V1.4.1717
minfi package	Bioconductor	https://doi.org/10.18129/B9.bioc.minfi
SeSAMe package	Bioconductor	https://doi.org/10.18129/B9.bioc.sesame
DunedinPACE package	Github	https://github.com/danbelsky/DunedinPACE
PC-Clocks package	Github	https://github.com/MorganLevineLab/PC-Clocks
Data underlying all plots	This study	Data S1

RESOURCE AVAILABILITY

Lead contact

Further information and requests for resources and reagents should be directed to and will be fulfilled by the lead contact, Vadim Gladyshev (vgladyshev@rics.bwh.harvard.edu).

Materials availability

Unique materials will be made available upon reasonable request to the lead contact.

Data and code availability

- All data originally generated in this study will be made available in GEO upon publication (see key resources table for accession numbers). Source data are provided in Data S1: Data underlying all plots.
- This paper does not report original code.
- Any additional information required to reanalyze the data reported in this paper is available from the lead contact upon request.

Please cite this article in press as: Poganik et al., Biological age is increased by stress and restored upon recovery, Cell Metabolism (2023), https://doi.org/10.1016/j.cmet.2023.03.015

EXPERIMENTAL MODEL AND SUBJECT DETAILS

Mouse experiments

All mouse experiments were approved by the Mass General Brigham IACUC or the Duke University IACUC. C57Bl/6 mice were obtained from Jackson Laboratories and acclimated to our animal facility for at least 48 h before being subjected to any experimental manipulation. Aged C57Bl/6 mice for parabiosis experiments were obtained from the NIA aged rodent colony. Mice were maintained in a barrier facility in sterilized, ventilated cages and fed standard laboratory chow (LabDiet 5053) and reverse osmosis drinking water ad libitum and maintained on a 12h:12h light:dark cycle. Mice were generally housed socially (5 mice/cage) except for the pregnancy studies wherein male mice were housed individually after mating. Mice were humanely euthanized at the conclusion of each experiment by CO_2 exposure followed by cervical dislocation.

Mouse parabiosis experiments

Parabiosis was carried out as previously described.[20] Female C57Bl/6 mice were pre-screened to minimize body size differences, and were randomly assigned to parabiosis pairs. Isochronic pairs consisted of two 3-month-old mice and heterochronic pairs consisted of one 3-month-old mouse and one 20-month-old mouse. Pairs were surgically attached and maintained for 3 months. Following 3 months of parabiosis, a subset of mice were euthanized for analysis and another subset were surgically separated. Fascia and skin were sutured closed following separation, and mice were allowed to recover for 2 months, after which they were for euthanized for analysis.

Mouse pregnancy experiments

C57Bl/6 mice (11 weeks old) were obtained from Jackson Laboratories. Three days before mating, male mice were separated into individual cages and soiled bedding from male cages was added to female cages to induce estrus.[60] 1:1 mating pairs were set up in the evening and left overnight. Females were removed from male cages the following morning and inspected for copulatory plugs. Pregnant females were identified by daily tracking of body weight. Blood was collected in EDTA tubes by submandibular vein puncture every two weeks to create a series of four samples per mouse: (1) 10 days before mating; (2) 4 days after mating; (3) 18 days after mating; and (4) 32 days after mating, generally corresponding to ~2 weeks postpartum. Pups were humanely euthanized shortly after birth allowing mothers to recover from pregnancy without needing to nurse. Blood was snap-frozen in liquid nitrogen immediately after collection and stored at –80°C until needed.

COVID-19 study

This study was approved by the Mass General Brigham IRB (protocol number 2020P004121). We selected a cohort of patients with RT-PCR-confirmed COVID-19 who were admitted to the intensive care units of Brigham and Women's Hospital (Boston, MA, USA). Clinical blood samples from these subjects were obtained through the Crimson Core facility of Mass General Brigham. Buffy coats from these blood samples were used as a source of DNA for methylation profiling as described elsewhere. Clinical and demographic data were collected by review of electronic medical records. Descriptive statistics are provided in Table 1.

METHOD DETAILS

Isolation of nucleic acids

DNA was isolated from human buffy coat samples at the Crimson Core facility (Mass General Brigham) using the QIAamp DNA Blood Mini Kit (Qiagen 51104) following the manufacturer's protocol. Eluted DNA was concentrated using a speedvac. DNA was isolated from mouse tissues using the DNeasy Blood and Tissue Kit (Qiagen) following the manufacturer's protocol. RNA was isolated from mouse tissues using the Ambion RNAqueous Total RNA Isolation Kit (Invitrogen). Generally, 50–100 μl of blood or ~25 mg of solid tissue was used as starting material. Concentration of DNA/RNA samples was determined using the Qubit dsDNA BR or RNA HS assay kit (Invitrogen). Isolated DNA was stored at –20°C and isolated RNA was stored at –80°C.

DNA methylation profiling

Methylation data was generated through the Epigenetic Clock Development Foundation. Human DNA samples for the COVID study were subjected to the Infinium MethylationEPIC array (Illumina) at AKESOgen Inc., and mouse DNA samples were subjected to the HorvathMammalMethylChip40 at the UCLA Neuroscience Genomic Core (UNGC). Samples were randomized to avoid introduction of batch/chip effects, but longitudinal samples from a single patient/mouse were run on the same chip. All sample preparation/processing was carried out according to the Illumina kit protocols.

Other sources of human methylation data

Illumina HumanMethylation450 BeadChip data for surgical patients from Sadahiro et al.[26] were downloaded from GEO (GSE142536). Illumina HumanMethylation450 BeadChip data for the Emory University African American Microbiome in Pregnancy Cohort are publicly available via GEO (GSE107459). In our study, only paired samples were analyzed; participants with only a single blood sample were excluded. Illumina HumanMethylation450 BeadChip data from Guintivano et al.[33] are publicly available via GEO (GSE44132). Chronological age data for this cohort were kindly provided by Prof. Zachary Kaminsky (The Royal, Canada). Illumina

MethylationEPIC BeadChip data from the Born into Life cohort[35,36] were kindly provided by Prof. Catarina Almqvist (Karolinska Institutet, Sweden). Detailed information for these datasets can be found in Table S2.

Gene expression profiling

Total RNA isolated as described above was checked for quality using an Agilent 2100 Bioanalyzer. Samples that passed QC were paired-end sequenced on an Illumina NovaSeq 6000 S4 with 100 bp read length.

Metabolite profiling

Metabolite profiling was carried out using a modified version of a reported procedure.[61] Portions of liver tissue from parabiosis animals were weighed, mixed with a volume of water equal to 4x the weight of the tissue, and homogenized for 4 min at 20Hz with 2x3mm tungsten beads in a Tissuelyser II (Qiagen). Samples were aliquoted in preparation for four orthogonal LC/MS profiling experiments: 10 ul portions each for hydrophobic interaction liquid chromatography (HILIC)-positive ionization mode and C8-positive ionization mode, and 30 ul portions for HILIC-negative ionization mode and C8-negative ionization mode. Further processing steps differed based on the profiling mode.

1. HILIC-pos profiling was carried out on a Shimadzu Nexera X2 U-HPLC (Shimadzu Corp.; Marlborough, MA) coupled to a Q Exactive hybrid quadrupole orbitrapmass spectrometer (Thermo Fisher Scientific; Waltham, MA). Protein was precipitated from samples by addition of nine volumes of 74.9:24.9:0.2 v/v/v acetonitrile/methanol/formic acid containing internal standards (valine-d8, Sigma-Aldrich; St. Louis, MO; and phenylalanine-d8, Cambridge Isotope Laboratories; Andover, MA). Precipitated material was cleared by centrifugation and the supernatant was injected directly onto a 150 × 2 mm 3 μm Atlantis HILIC column (Waters; Milford, MA). Elution was as follows: (1) 5% mobile phase A (10 mM ammonium formate and 0.1% formic acid in water), 0.5 min, 250 μL/min; (2) linear gradient to 40% mobile phase B (acetonitrile with 0.1% formic acid), 10 min, 250 μL/min. MS analysis was with electrospray ionization (ESI) in positive ion mode with the following parameters: full scan analysis over 70–800 m/z at 70,000 resolution and 3 Hz data acquisition rate; sheath gas 40; sweep gas 2; spray voltage 3.5 kV; capillary temperature 350°C; S-lens RF 40; heater temperature 300°C; microscans 1; automatic gain control target 1e6; and maximum ion time 250 ms.
2. HILIC-neg profiling was carried out on an AQUITY UPLC system (Waters; Milford, MA coupled to a 5500 QTRAP mass spectrometer (SCIEX; Framingham, MA). Protein was precipitated from samples by addition of four volumes of 80% methanol containing internal standards (inosine-15N4, thymine-d4 and glycocholate-d4; Cambridge Isotope Laboratories; Andover, MA). Precipitated material was cleared by centrifugation and the supernatant was injected directly onto a 150 × 2.0 mm Luna NH2 column (Phenomenex; Torrance, CA). Elution was as follows: (1) 10% mobile phase A (20 mM ammonium acetate and 20 mM ammonium hydroxide in water) and 90% mobile phase B (10 mM ammonium hydroxide in 75:25 v/v acetonitrile/methanol), 400 μL/min; (2) linear gradient to 100% mobile phase A, 10 min, 400 μL/min. MS analysis was with ESI and selective multiple reaction monitoring scans in the negative ion mode[61] with the following parameters: ion spray voltage −4.5 kV; source temperature 500°C.
3. C8-pos profiling was carried out on a Shimadzu Nexera X2 U-HPLC (Shimadzu Corp.; Marlborough, MA) coupled to a Exactive Plus orbitrap mass spectrometer (Thermo FisherScientific; Waltham, MA). Lipids were extracted from samples by addition of 190 μL isopropanol containing 1,2-didodecanoyl-sn-glycero-3-phosphocholine (Avanti Polar Lipids; Alabaster, AL). Insoluble material was cleared by centrifugation and the supernatant was injected directly onto a 100 × 2.1 mm, 1.7 μm ACQUITY BEH C8 column (Waters; Milford, MA). Elution was as follows: (1) 80% mobile phase A (95:5:0.1 vol/vol/vol 10mM ammonium acetate/methanol/formic acid), 1 min; (2) linear gradient to 80% mobile- phase B (99.9:0.1 vol/vol methanol/formic acid), 2 min; (3) linear gradient to 100% mobile phase B, 7 min; (4) 100% mobile-phase B, 3 min. MS analysis was with ESI in positive ion mode with the following parameters: full scan analysisover 200–1000 m/z at 70,000 resolution and 3 Hz data acquisition rate; sheath gas 50; in source CID 5 eV; sweep gas 5; spray voltage 3 kV; capillary temperature 300°C; S-lens RF 60; heater temperature 300°C; microscans 1; automatic gain control target 1e6; and maximum ion time 100 ms.
4. C8-neg profiling was carried out on a Shimadzu Nexera X2 U-HPLC (Shimadzu Corp.;Marlborough, MA) coupled to a Q Exactive hybrid quadrupole orbitrap mass spectrometer (Thermo Fisher Scientific; Waltham, MA). Free fatty acids and bile acids were extracted from samples by addition of 90 μL methanol containing PGE2-d4 (Cayman Chemical Co.; Ann Arbor, MI). Elution was as follows: (1) 60% mobile phase A (0.1% formic acid in water), 4 min, 400 μL/min; (2) linear gradient to 100% mobile phase B (acetonitrile with 0.1% formic acid), 8 min. MS analysis was with ESI in negative ion mode with the following parameters: full scan MS acquisition over 200–550 m/z at 70,000 resolution; sheath gas 45; sweep gas 5; spray voltage −3.5 kV; capillary temperature 320°C; S- lens RF 60; heater temperature 300°C; microscans 1; automatic gain control target 1e6; and maximum ion time 250 ms.

Raw data was processed using TraceFinder (Thermo Fisher Scientific; Waltham, MA) and Progenesis QI (Nonlinear Dynamics; Newcastle upon Tyne, UK) for Q Exactive (Plus) experiments or MultiQuant (SCIEX; Framingham, MA) for 5500 QTRAP experiments. Metabolite identities were confirmed using authentic reference standards or reference samples. Insoluble material was cleared by centrifugation and the supernatant was injected directly onto a 150 × 2 mm ACQUITY T3 column (Waters; Milford, MA).

Please cite this article in press as: Poganik et al., Biological age is increased by stress and restored upon recovery, Cell Metabolism (2023), https://doi.org/10.1016/j.cmet.2023.03.015

QUANTIFICATION AND STATISTICAL ANALYSIS

DNAm clock analysis

For mammalian microarray analysis, raw methylation data were first normalized using the SeSAMe R package and beta values were calculated. DNAm age biomarkers were calculated as previously described.[9] For publicly available human datasets, if raw idat methylation files were available, they were processed using the minfi R package.[62] Data were first preprocessed using noob normalization and then beta values were calculated using the getBeta function. For datasets where only raw or normalized methylation data/calculated beta values were the only data available, these data were used directly. Human DNAm age biomarkers were calculated using the online Hovath DNA Methylation Age Calculator, which calculates Horvath DNAm age,[6] Hannum DNAm age,[7] Skin & Blood DNAm age,[8] DNAmPhenoAge,[14] and DNAmGrimAge,[15] among other parameters. DunedinPACE[17] was calculated with the DunedinPACE R package.[63] RRBS-based epigenetic clocks were applied as previously described.[10,11,20] PC clocks were applied using publicly available code.[28]

DNAm age analysis

All DNAm age biomarkers were adjusted by chronological age to yield an age acceleration parameter. For human studies, this was carried out by calculating residuals from regressing DNAm age on chronological age. Note that this correction is neither necessary nor relevant for DunedinPACE. For mouse experiments, linear regressions are skewed by the strong effects of the experimental interventions applied (e.g. parabiosis). Thus, for mouse experiments, we calculated age acceleration by subtracting chronological age from DNAm age.

In one case (the White et al. human pregnancy dataset), chronological ages were not available. To account for the passage of time in this longitudinal dataset, we corrected the DNAm age predictions by the average amount of time between each sample collection point, based on the methods of the original publication[32] and the assumption that most women do not learn they are pregnant for 6 weeks on average. This corresponded to the following time corrections: 0.26, 0.635, and 0.75 years, respectively, for time points 2, 3, and 4.

Gene expression analysis

For RNAseq data, we filtered out genes with low number of reads, keeping only the genes with at least 10 reads in at least 50% of the samples, which resulted in 12,374 detected genes according to Entrez annotation. Filtered data was then passed to RLE normalization.[64] Differential expression of genes in response to heterochronic parabiosis compared to isochronic parabiosis was analyzed using edgeR[65] separately for merged and detached models. Obtained p-values were adjusted for multiple comparison with Benjamini-Hochberg method.[66]

Association with gene expression signatures

Association of gene expression log-fold changes induced by heterochronic parabiosis with previously established transcriptomic signatures of aging was examined as described in Tyshkovskiy et al.[23] separately for merged and detached groups. Liver-specific and multi-tissue mouse signatures obtained via a meta-analysis of age-related gene expression changes from multiple datasets were utilized for this analysis.

First, for every signature we specified 250 genes with the lowest p-values and divided them into up- and downregulated genes. These lists were subsequently considered as gene sets. Then, we ranked genes differentially expressed in response to heterochronic parabiosis based on their p-values, calculated as described above. Afterwards, we utilized gene set enrichment analysis (GSEA)[67] to calculate normalized enrichment scores (NES) separately for up- and downregulated lists of gene sets as described in Tyshkovskiy et al.,[23] and calculated the final NES as a mean of the two. To calculate statistical significance of obtained NES, we performed permutation testing where we randomly assigned genes to the lists of gene sets, maintaining their size. To get the p-value of the association between parabiosis and a certain signature, we used 5,000 permutations and calculated the frequency of random final NES that are larger in magnitude than the observed final NES. To adjust for multiple testing, we performed a Benjamini-Hochberg correction. Final NES for association of response to heterochronic parabiosis with aging signatures were used to generate barplots.

Functional enrichment analysis

For the identification of enriched functions distinguishing isochronic and heterochronic mice, we performed functional GSEA[67] on a pre-ranked list of genes based on $\log_{10}$(p-value) corrected by the sign of regulation, calculated as:

$$-(pv) \times sgn(lfc),$$

where *pv* and *lfc* are p-value and logFC of a certain gene, respectively, obtained from edgeR output, and *sgn* is the signum function (equal to 1, -1 and 0 if value is positive, negative or equal to 0, respectively). REACTOME, KEGG and HALLMARK ontologies from the Molecular Signature Database (MSigDB) were used as gene sets for GSEA. The GSEA algorithm was performed separately for merged and detached models via the *fgsea* package in R with 5000 permutations. A q-value cutoff of 0.1 was used to select statistically significant functions.

Similar analysis was performed for gene expression signatures of aging. Pairwise Spearman correlation was calculated for individual signatures of heterochronic parabiosis and aging based on estimated NES. A heatmap colored by NES was built for manually

chosen statistically significant functions (adjusted p-value < 0.1). Complete list of functions enriched by at least one signature of heterochronic parabiosis is included in Table S1.

Metabolomics analysis

Metabolomics data was analyzed using MetaboAnalyst.[68] Normalized data were mean-centered and auto-scaled. Age-related metabolites were defined as those which significantly changed (FDR threshold 0.1) between old and young isochronic parabionts. Both attached and detached animals were compared, and the intersecting set of metabolites was used for further analysis. To evaluate the effect of heterochronic parabiosis on metabolite levels, metabolites showing less than 10% fold change were first filtered, then the fold changes of age-related metabolites was compared between the indicated parabiosis condition (Figures 2C and 2D) and between old and young isochronic animals. Kendall correlation was used to calculate correlation coefficients and p values.

Differential methylation analysis

Differential methylation modeling was carried out using SeSAMe.[69] The following comparisons were made for models of stress: Emory pregnancy, time point 2 vs. time point 1; Surgery, time point 2 vs. time point 1; Guintivano et al. pregnancy, trimester 3 vs. trimester 1. The following comparisons were made for models of recovery: COVID infection, female patients: time point 4 vs. time point 1; Surgery, time point 3 vs. time point 2; White et al.pregnancy, time point 4 vs. time point 3. CpGs were considered significantly differentially methylated if adjusted p value was less than 0.05. CpGs with increasing methylation levels were separated from those with decreasing methylation levels, and intersections between the various models were used to construct the Venn diagrams in Figure S6.

Statistics

For longitudinal datasets, repeated measures ANOVA or mixed effects models were first used to test for significant variance between time points. If these tests revealed a significant effect, paired t tests corrected by controlling the false discovery rate using the Benjamini-Hochberg method were carried out between groups. Exact p values are shown within all figures. For non-longitudinal datasets, a similar procedure was used except that traditional ANOVAs and unpaired t tests were used. All t tests were two-tailed. Sample sizes are indicated in figure legends.

Cell Metabolism, Volume *35*

Supplemental information

Biological age is increased by stress and restored upon recovery

Jesse R. Poganik, Bohan Zhang, Gurpreet S. Baht, Alexander Tyshkovskiy, Amy Deik, Csaba Kerepesi, Sun Hee Yim, Ake T. Lu, Amin Haghani, Tong Gong, Anna M. Hedman, Ellika Andolf, Göran Pershagen, Catarina Almqvist, Clary B. Clish, Steve Horvath, James P. White, and Vadim N. Gladyshev

Supplemental Information For

Biological age is increased by stress and restored upon recovery

Jesse R. Poganik,[1] Bohan Zhang,[1] Gurpreet S. Baht,[2,3] Alexander Tyshkovskiy,[1] Amy Deik,[4] Csaba Kerepesi,[1] Sun Hee Yim,[1] Ake T. Lu,[5,6] Amin Haghani,[5,6] Tong Gong,[7] Anna M. Hedman,[7] Ellika Andolf,[8] Göran Pershagen,[9,10] Catarina Almqvist,[7,11] Clary B. Clish,[4] Steve Horvath,[5,6,12] and James P. White,[2,3*] and Vadim N. Gladyshev[1*†]

[1]Division of Genetics, Department of Medicine, Brigham and Women's Hospital, Harvard Medical School, Boston, MA 02115, USA.
[2]Department of Medicine, Duke University School of Medicine, Durham, NC 27701, USA.
[3]Duke Molecular Physiology Institute, Duke University, Durham, NC 27701, USA.
[4]Broad Institute of MIT and Harvard, Cambridge, MA 01241, USA.
[5]Department of Human Genetics, David Geffen School of Medicine, University of California, Los Angeles, Los Angeles, CA 90095, USA.
[6]Altos Labs, San Diego, CA, USA.
[7]Department of Medical Epidemiology and Biostatistics, Karolinska Institutet, Stockholm, Sweden.
[8]Department of Clinical Sciences, Division of Obstetrics and Gynaecology, Danderyd Hospital, Karolinska Institutet, Stockholm, Sweden.
[9]Institute of Environmental Medicine, Karolinska Institutet, Stockholm, Sweden.
[10]Centre for Occupational and Environmental Medicine, Region Stockholm, Stockholm, Sweden.
[11]Astrid Lindgren Children's Hospital, Karolinska University Hospital, Stockholm, Sweden.
[12]Department of Biostatistics, School of Public Health, University of California, Los Angeles, Los Angeles, CA 90095, USA.

[†]Lead contact
[*]Corresponding authors: vgladyshev@rics.bwh.harvard.edu (VNG) and james.white@duke.edu (JPW)

Contents:

Supplemental Figures 2
Supplemental Tables 12
Supplemental References 13

Supplemental Figures

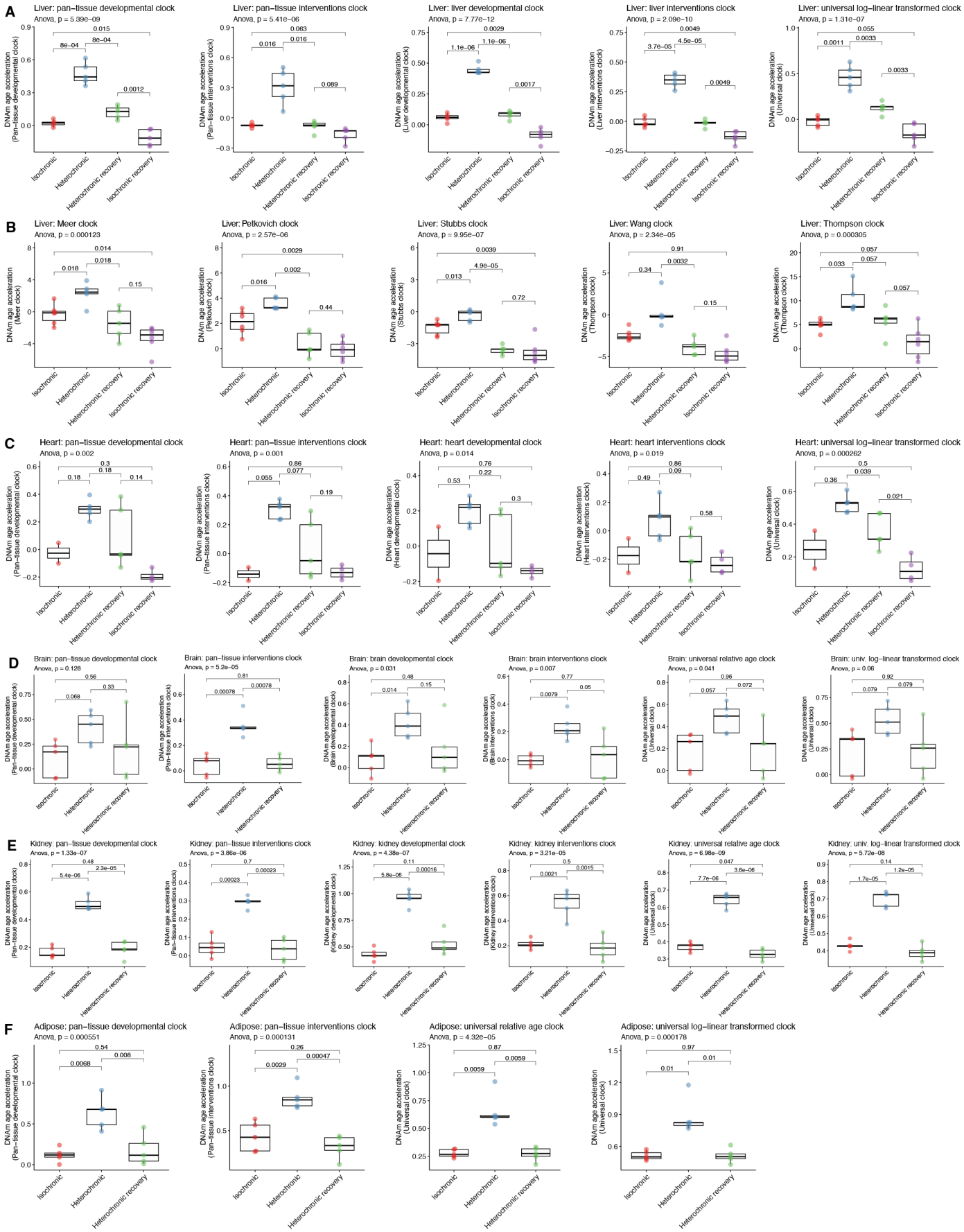

Figure S1. Additional clocks applied to heterochronic parabionts, related to Figure 1. (A) DNAm age predictions from the HorvathMammalMethyl40 array and related clocks [1] including the pan-tissue developmental and interventions clocks, the liver developmental and interventions clocks, and the log-linear transformed universal pan-mammalian clock. (B) DNAm age acceleration results from RRBS-based DNAm clocks, including those of Meer *et al.,*[2] Petkovich *et al.,*[3] Stubbs *et al.,*[4] Wang *et al.,*[5] and Thompson *et al.*[6] (C) DNAm age predictions from the HorvathMammalMethyl40 array and related clocks applied to heart tissue including the pan-tissue developmental and interventions clocks, the heart developmental and interventions clocks, and the log-linear transformed universal pan-mammalian clock.(D) DNAm age predictions from the HorvathMammalMethyl40 array and related clocks applied to brain tissue including the pan-tissue developmental and interventions clocks, the brain developmental and interventions clocks, and the log-linear transformed universal pan-mammalian clock. (E) DNAm age predictions from the HorvathMammalMethyl40 array and related clocks applied to kidney tissue including the pan-tissue developmental and interventions clocks, the kidney developmental and interventions clocks, and the log-linear transformed universal pan-mammalian clock. (F) DNAm age predictions from the HorvathMammalMethyl40 array and related clocks applied to adipose tissue including the pan-tissue developmental and interventions clocks, the relative age universal pan-mammalian clock, and the log-linear transformed universal pan-mammalian clock. P values were calculated with ANOVA and unpaired t-tests. Sample sizes: A–B, n= 6 for isochronic and isochronic recovery, and n=5 for heterochronic and heterochronic recovery; C, n=5 for heterochronic and heterochronic recovery, n=2 for isochronic, and n=4 for isochronic recovery; D–F, n=5 for all conditions.

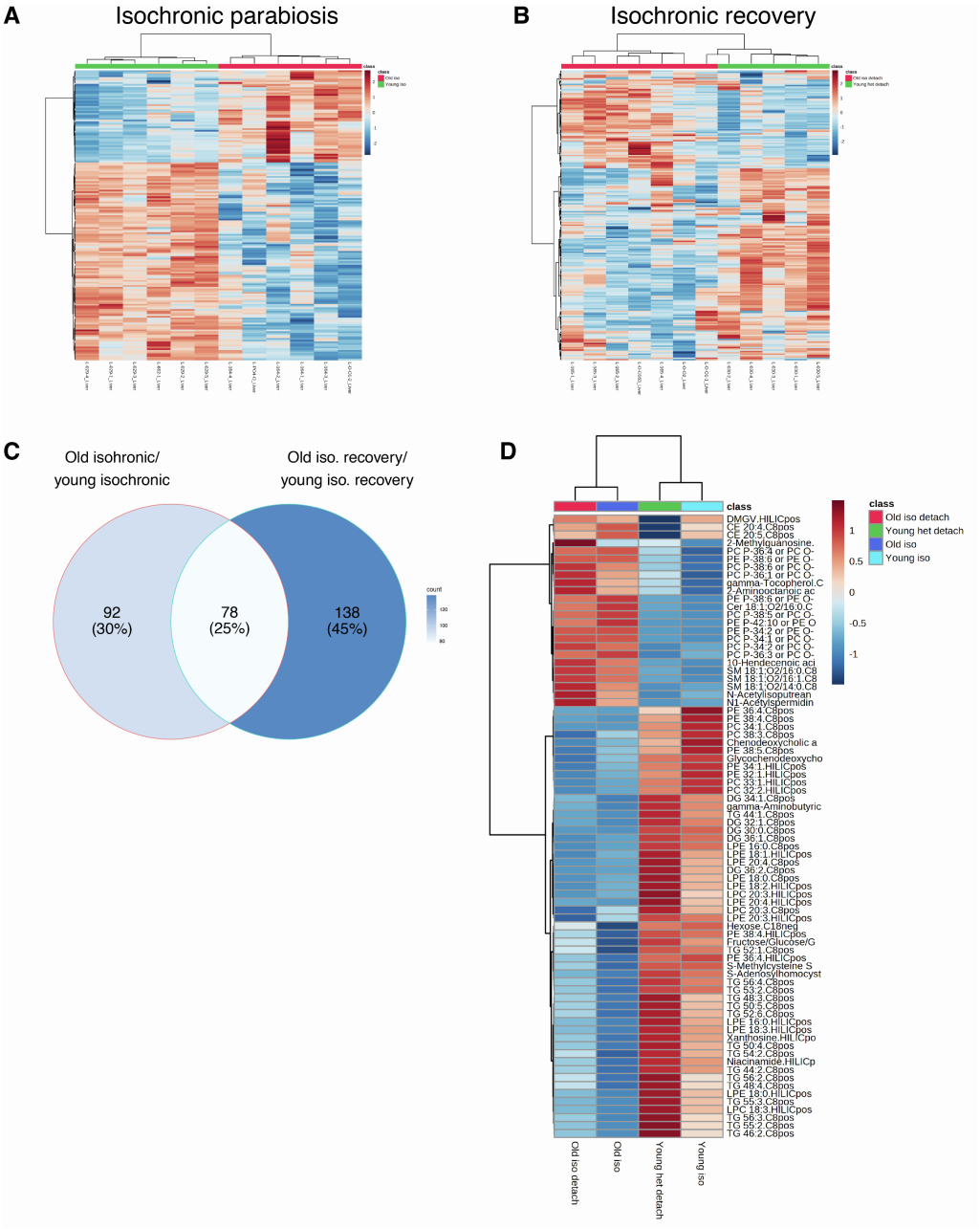

Figure S2. Identification of age-related metabolites, related to Figure 2. (A–B) Heatmap of metabolites found to be significantly differentially abundant in livers of old and young isochronic parabionts during parabiosis (A) and upon recovery (B). (C) The 78 common metabolites between these two sets were considered age-related metabolites and were used for further study. (D) Heatmap of the 78 age-related metabolites across conditions. Sample sizes: young isochronic, n=6; old isochronic, n=6; young isochronic recovery, n=5; old isochronic recovery, n=7.

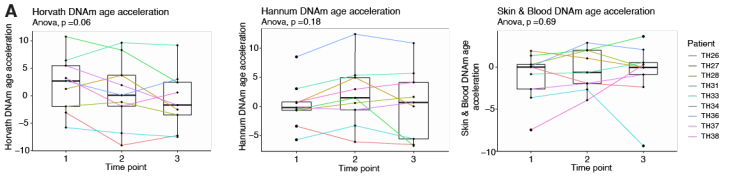
A
Horvath DNAm age acceleration
Anova, p =0.06
Hannum DNAm age acceleration
Anova, p =0.18
Skin & Blood DNAm age acceleration
Anova, p =0.69
Horvath DNAm age acceleration
Hannum DNAm age acceleration
Skin & Blood DNAm age acceleration
Time point
Patient
TH26
TH27
TH28
TH31
TH33
TH34
TH36
TH37
TH38

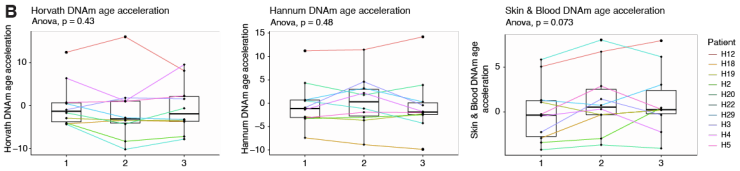
B
Horvath DNAm age acceleration
Anova, p = 0.43
Hannum DNAm age acceleration
Anova, p = 0.48
Skin & Blood DNAm age acceleration
Anova, p = 0.073
Horvath DNAm age acceleration
Hannum DNAm age acceleration
Skin & Blood DNAm age acceleration
Time point
Patient
H12
H18
H19
H2
H20
H22
H29
H3
H4
H5

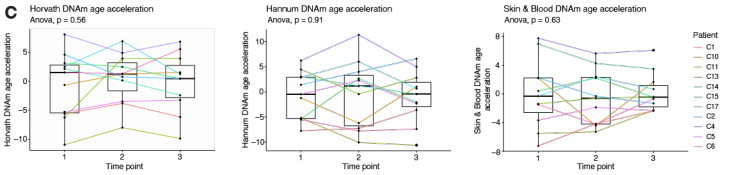
C
Horvath DNAm age acceleration
Anova, p = 0.56
Hannum DNAm age acceleration
Anova, p = 0.91
Skin & Blood DNAm age acceleration
Anova, p = 0.63
Horvath DNAm age acceleration
Hannum DNAm age acceleration
Skin & Blood DNAm age acceleration
Time point
Patient
C1
C10
C11
C13
C14
C15
C17
C2
C4
C5
C6

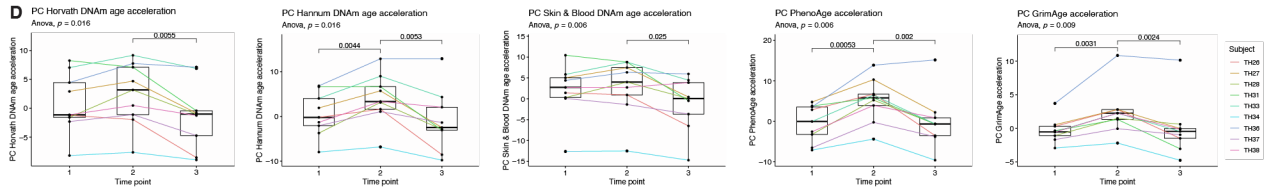
D
PC Horvath DNAm age acceleration
Anova, p = 0.016
PC Hannum DNAm age acceleration
Anova, p = 0.016
PC Skin & Blood DNAm age acceleration
Anova, p = 0.006
PC PhenoAge acceleration
Anova, p = 0.006
PC GrimAge acceleration
Anova, p = 0.009
0.0055
0.0044
0.0053
0.025
0.00053
0.002
0.0031
0.0024
PC Horvath DNAm age acceleration
PC Hannum DNAm age acceleration
PC Skin & Blood DNAm age acceleration
PC PhenoAge acceleration
PC GrimAge acceleration
Time point
Subject
TH26
TH27
TH28
TH31
TH33
TH34
TH36
TH37
TH38

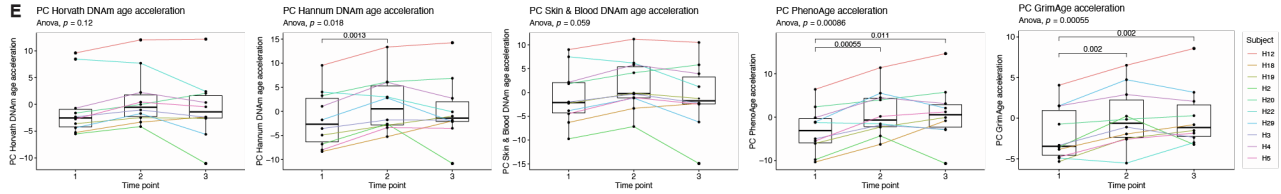
E
PC Horvath DNAm age acceleration
Anova, p = 0.12
PC Hannum DNAm age acceleration
Anova, p = 0.018
PC Skin & Blood DNAm age acceleration
Anova, p = 0.059
PC PhenoAge acceleration
Anova, p = 0.00086
PC GrimAge acceleration
Anova, p = 0.00055
0.0013
0.00055
0.011
0.002
0.002
PC Horvath DNAm age acceleration
PC Hannum DNAm age acceleration
PC Skin & Blood DNAm age acceleration
PC PhenoAge acceleration
PC GrimAge acceleration
Time point
Subject
H12
H18
H19
H2
H20
H22
H29
H3
H4
H5

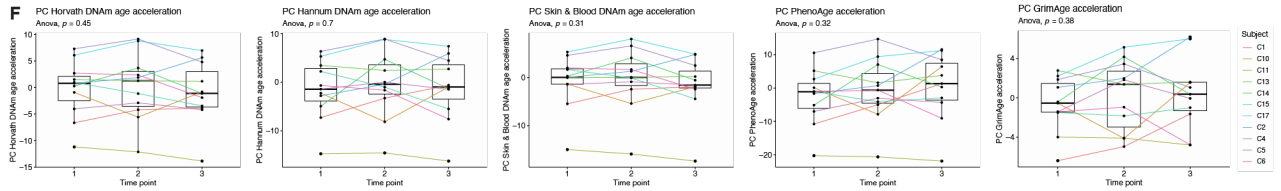
F
PC Horvath DNAm age acceleration
Anova, p = 0.45
PC Hannum DNAm age acceleration
Anova, p = 0.7
PC Skin & Blood DNAm age acceleration
Anova, p = 0.31
PC PhenoAge acceleration
Anova, p = 0.32
PC GrimAge acceleration
Anova, p = 0.38
PC Horvath DNAm age acceleration
PC Hannum DNAm age acceleration
PC Skin & Blood DNAm age acceleration
PC PhenoAge acceleration
PC GrimAge acceleration
Time point
Subject
C1
C10
C11
C13
C14
C15
C17
C2
C4
C5
C6

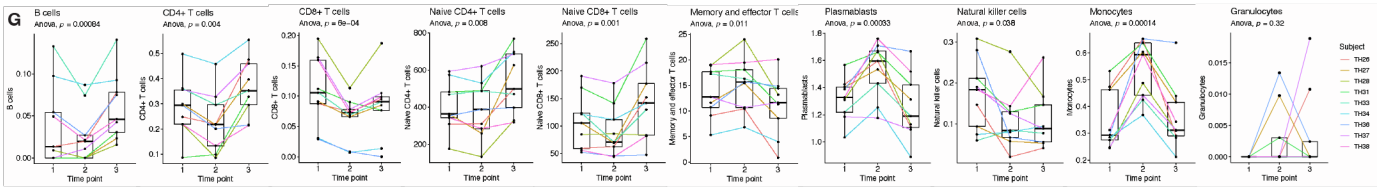
G
B cells
Anova, p = 0.00084
CD4+ T cells
Anova, p = 0.004
CD8+ T cells
Anova, p = 9e-04
Naive CD4+ T cells
Anova, p = 0.008
Naive CD8+ T cells
Anova, p = 0.001
Memory and effector T cells
Anova, p = 0.011
Plasmablasts
Anova, p = 0.00033
Natural killer cells
Anova, p = 0.038
Monocytes
Anova, p = 0.00014
Granulocytes
Anova, p = 0.32
Time point
Subject
TH26
TH27
TH28
TH31
TH33
TH34
TH36
TH37
TH38

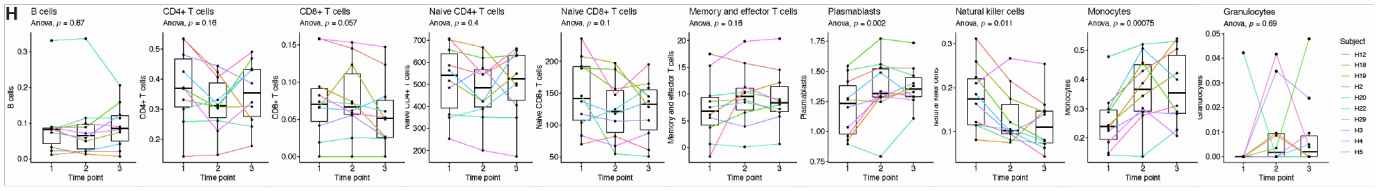
H
B cells
Anova, p = 0.87
CD4+ T cells
Anova, p = 0.16
CD8+ T cells
Anova, p = 0.057
Naive CD4+ T cells
Anova, p = 0.4
Naive CD8+ T cells
Anova, p = 0.1
Memory and effector T cells
Anova, p = 0.16
Plasmablasts
Anova, p = 0.002
Natural killer cells
Anova, p = 0.011
Monocytes
Anova, p = 0.00075
Granulocytes
Anova, p = 0.69
Time point
Subject
H12
H18
H19
H2
H20
H22
H29
H3
H4
H5

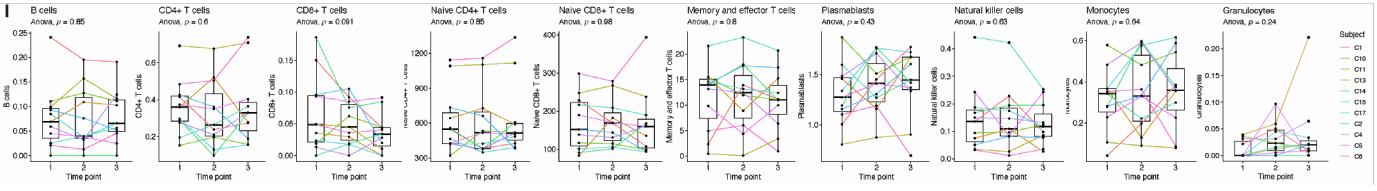
I
B cells
Anova, p = 0.85
CD4+ T cells
Anova, p = 0.6
CD8+ T cells
Anova, p = 0.091
Naive CD4+ T cells
Anova, p = 0.85
Naive CD8+ T cells
Anova, p = 0.98
Memory and effector T cells
Anova, p = 0.8
Plasmablasts
Anova, p = 0.43
Natural killer cells
Anova, p = 0.63
Monocytes
Anova, p = 0.64
Granulocytes
Anova, p = 0.24
Time point
Subject
C1
C10
C11
C13
C14
C15
C17
C2
C4
C5
C6

Figure S3. Additional DNAm parameters calculated for patients undergoing major surgery, related to Figure 3. (A–C) First generation DNAm age acceleration results for patients undergoing emergency surgery to repair traumatic hip fractures (A), elective hip replacement (B), and elective colorectal surgery (C) calculated using Horvath DNAm age,[7] Hannum DNAm age,[8] and Skin & Blood DNAm age[9]. (D–F) Principal component (PC) clocks results for patients undergoing emergency hip surgery (D), elective hip replacement (E), or elective colorectal surgery (F). (G–I) Predicted blood cell counts based on methylation data of patients undergoing emergency hip surgery (G), elective hip replacement (H), or elective colorectal surgery (I). Houseman[10] and Horvath/Levine[11] predictors of the indicated blood cell types were used to analyze blood composition dynamics in patients undergoing the indicated surgeries. In all panels, time point 1 corresponds to immediately before surgery; time point 2 corresponds to the morning after surgery; and time point 3 corresponds to the day of discharge from the hospital, 4–7 days post-surgery. P values were calculated with repeated-measures ANOVA and paired t-tests. Sample sizes: A, D, G, n=9; B, E, H, n=10; C, F, I, n=11.

Guintivano *et al.* 2014

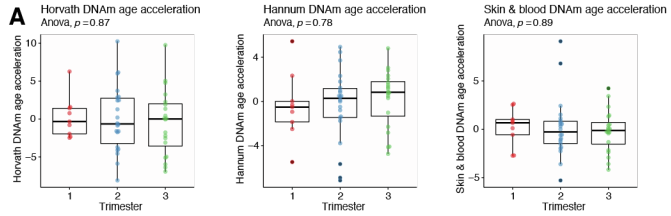

Emory Pregnancy Cohort

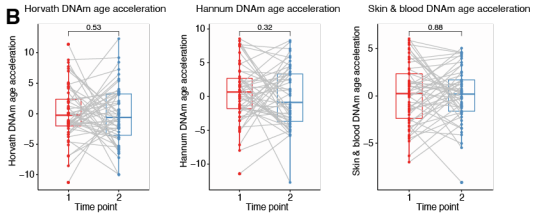

Born into Life Cohort

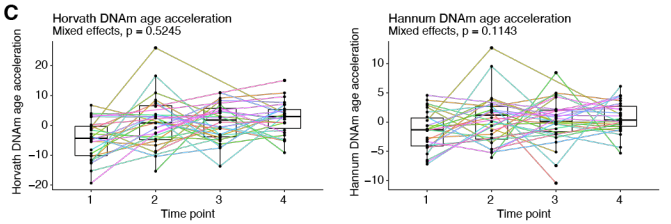

White *et al.* 2012

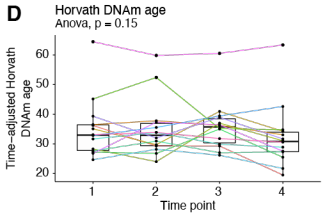

Guintivano *et al.* 2014

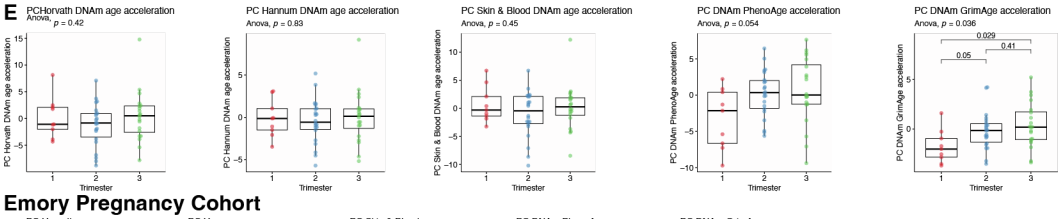

Emory Pregnancy Cohort

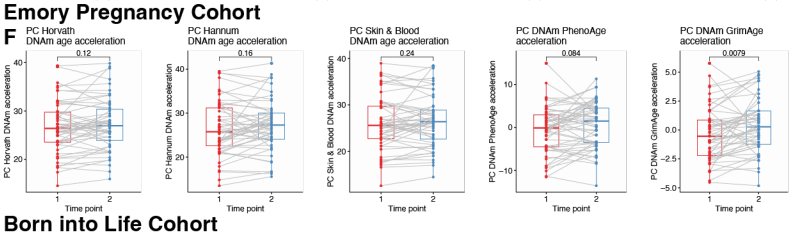

Born into Life Cohort

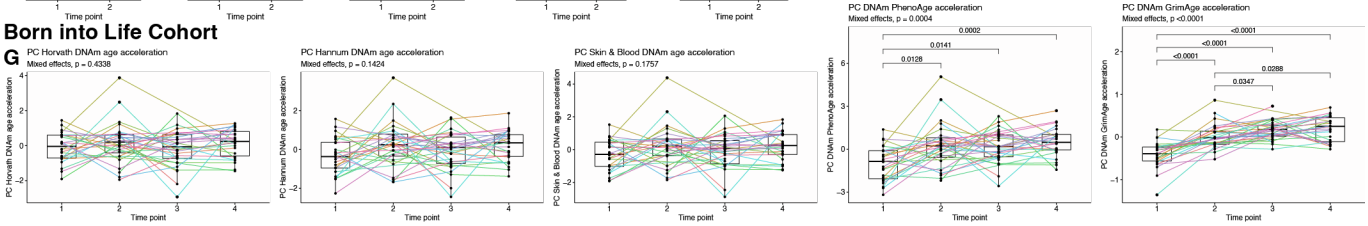

Guintivano *et al.* 2014

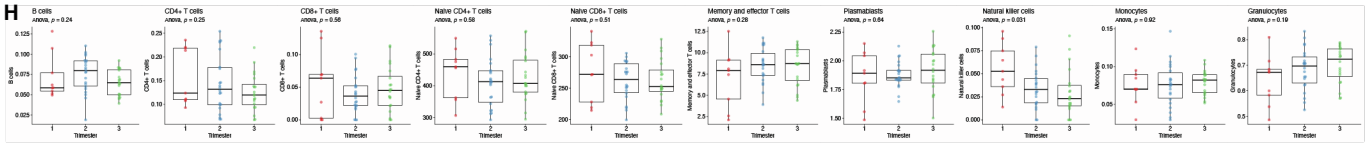

Emory Pregnancy Cohort

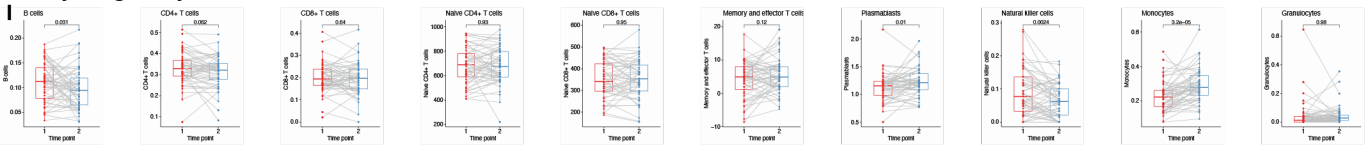

Born into Life Cohort

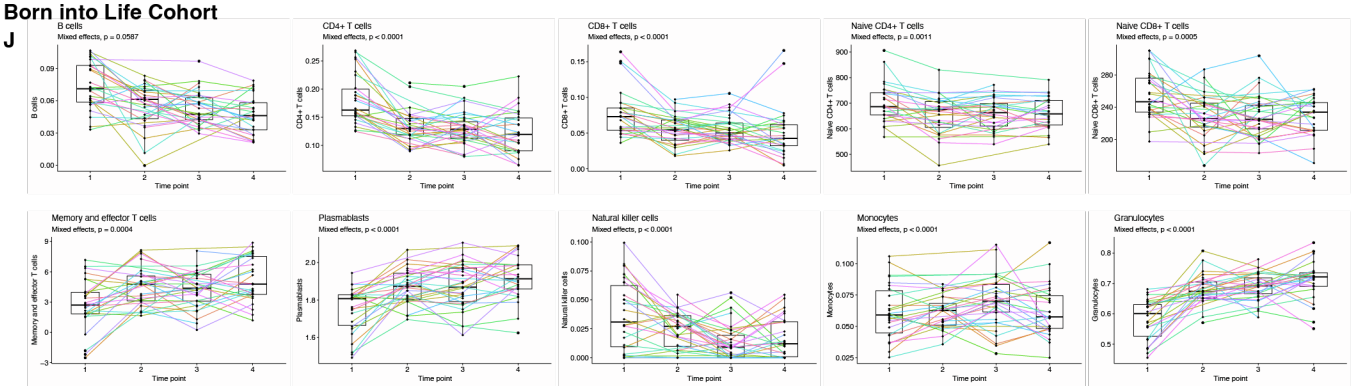

Figure S4. Additional DNAm parameters calculated for human pregnancy datasets, related to Figure 4. (A) Cross-sectional DNAm age acceleration analysis of pregnant Americans across the three trimesters of pregnancy using Horvath DNAm age, Hannum DNAm age, and Skin & Blood DNAm age. (B) DNAm age biomarkers (as in A) for a longitudinal study of pregnant African Americans with two blood samples collected over the course of pregnancy. Time point 1 corresponds to 7–15 weeks of pregnancy; time point 2 corresponds to 24–32 weeks of pregnancy. (C) DNAm age biomarkers (as in A–B) for Swedish mothers longitudinally tracked over the course of pregnancy. Time point 1 corresponds to pre-pregnancy; time point 2 corresponds to 10–14 weeks of pregnancy; time point 3 corresponds to 26–28 weeks of pregnancy; time point 4 corresponds to 2–4 days postpartum. (D) Horvath DNAm age (adjusted for the passage of time; see Methods for details) for a cohort of American mothers longitudinally tracked over the course of pregnancy and postpartum. Time point 1 corresponds to early pregnancy; time point 2 corresponds to mid-pregnancy; time point 3 corresponds to delivery; time point 4 corresponds to 6 weeks postpartum. (E–G) Principal component (PC) clocks results for human pregnancy cohorts. PC clocks (Horvath DNAm age, Hannum DNAm age, Skin & Blood DNAm age, DNAm PhenoAge, and DNAm GrimAge) were applied to methylation data from human pregnancy cohorts. Time points for each dataset are as defined above. (H–J) Predicted blood cell counts based on methylation data of human pregnancy cohorts. Houseman and Horvath/Levine predictors of the indicated blood cell types were used to analyze blood composition dynamics during human pregnancy. Time points for each dataset are as defined above. P values were calculated with ANOVA (A, E, H), repeated-measures ANOVA (D), unpaired t-tests (A, E, H), paired t-tests (B, F, I), and/or mixed effects models (C, G, J). Sample sizes: A, E, H, n=9, 22, and 20 for trimesters 1, 2, and 3, respectively; B, F, I n=53; C, G, J, n=33 total subjects who each provided up to 4 samples; D, n=14.

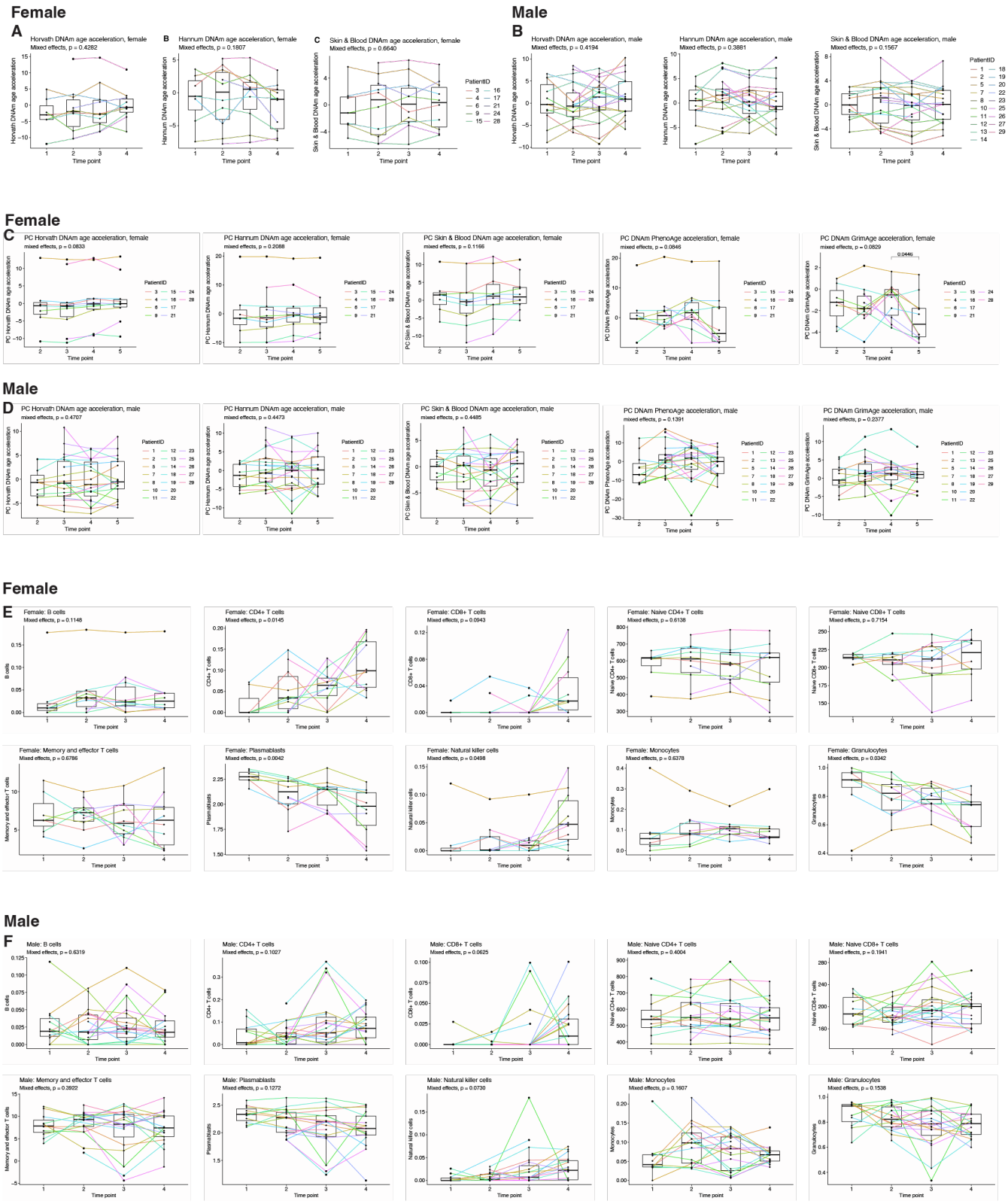

Figure S5. Additional DNAm parameters calculated for patients with COVID-19, related to Figure 5. (A–B) DNAm age acceleration results for Horvath DNAm age, Hannum DNAm age, and Skin & Blood DNAm age for females (A) and males (B). (C–D) Principal component (PC) clocks results for COVID-19 patients. PC clocks (Horvath DNAm age, Hannum DNAm age, Skin & Blood DNAm age, DNAm PhenoAge, and DNAm GrimAge) were applied to methylation data from COVID-19 patients. (E–F) Predicted blood cell counts based on methylation data of COVID-19 patients. Houseman and Horvath/Levine predictors of the indicated blood cell

types were used to analyze blood composition dynamics during COVID-19 disease. In all panels, Time point 1 is within 5 days ICU admission; time point 2 is within 5 days of the midpoint of the ICU stay; time point 3 is within 5 days of the date of discharge from the ICU; timepoint 4 is ≥7 days post-ICU discharge. P values were calculated using a mixed effects model with post-hoc pairwise comparison testing. Sample sizes: all panels, n=10 female and n=19 male subjects total who each provided up to 4 samples.

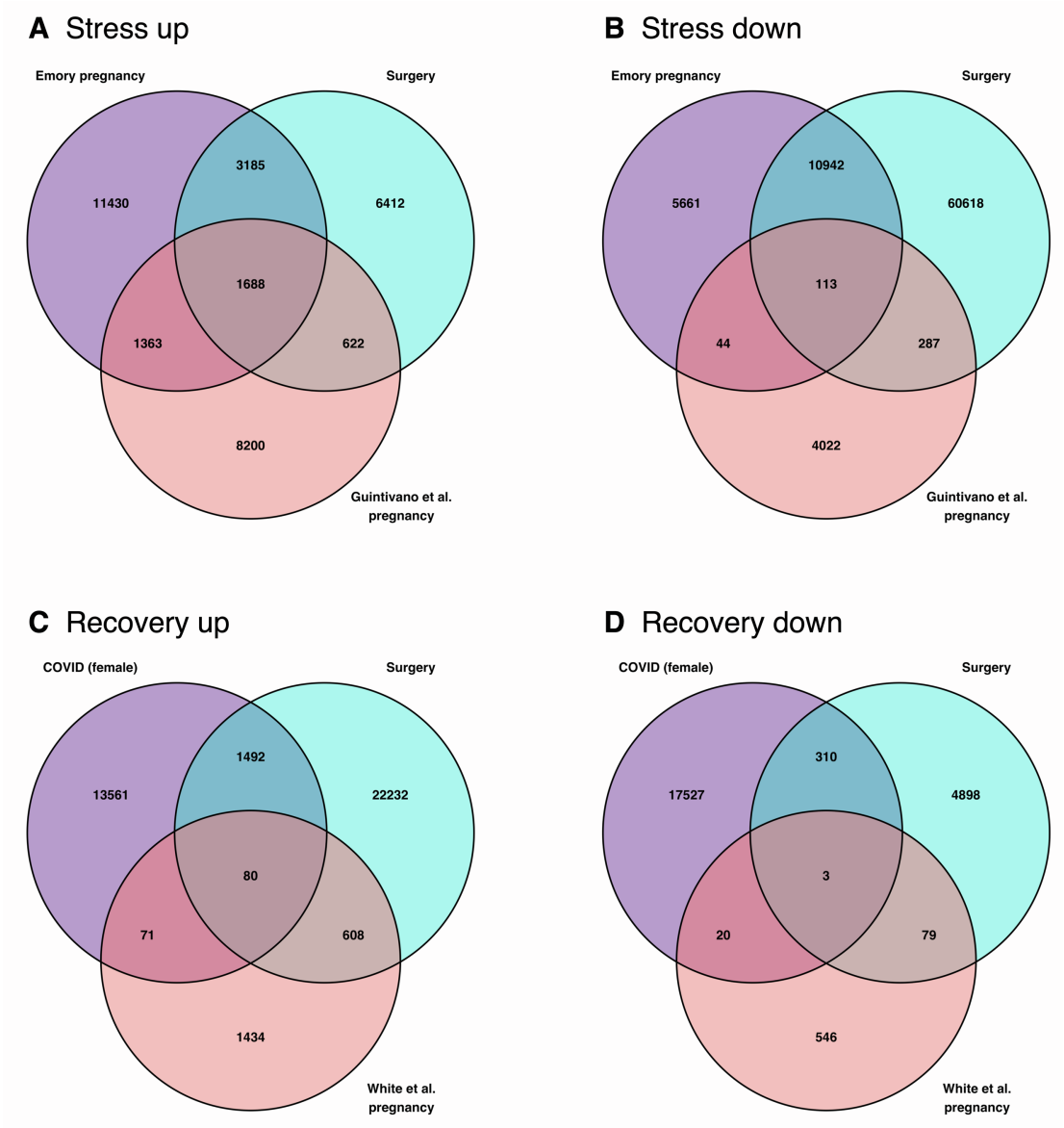

Figure S6. Identification of CpGs with common behavior across stress models, related to Figures 3–5. (A–B) CpGs that gain (A) or lose (B) methylation upon exposure to stress. (C–D) CpGs that gain (C) or lose (D) methylation upon recovery from stress. CpGs are listed in Table S3.

Supplemental Tables

Table S2. Sources of human DNA methylation data, related to Figures 3–5.

Dataset	Source	Description	Description of samples/time points:	Methylation array
Sadahiro *et al.* 2020[12]	GEO: GSE142536	Longitudinal study of elderly adults undergoing major surgery	1. Before surgery 2. Morning after surgery 3. Day of discharge from hospital (4–7 days post-surgery)	Illumina HumanMethylation450 BeadChip
Guintivano *et al.* 2014[13]	GEO: GSE44132	Cross-sectional study of pregnant women	Cross-sectional design with one sample per participant taken during a particular trimester	Illumina HumanMethylation450 BeadChip
Emory pregnancy cohort [14]	GEO: GSE107459	Longitudinal study of pregnant women	1. 7–15 weeks of pregnancy 2. 24–32 weeks of pregnancy	Illumina HumanMethylation450 BeadChip
Born into Life cohort [15,16]	Prof. Catarina Almqvist, Karolinska Institutet, Sweden	Longitudinal study of pregnant women	1. Pre-pregnancy 2. 10–14 weeks of pregnancy 3. 26–28 weeks of pregnancy 4. 2–4 days postpartum	Illumina MethylationEPIC BeadChip
White *et al.* 2012[17]	GEO: GSE37722	Longitudinal study of pregnant women	1. Early pregnancy 2. Mid-pregnancy 3. Delivery 4. 6 weeks postpartum	Illumina HumanMethylation27 BeadChip
COVID-19	This study	Longitudinal study of patients undergoing intensive care for COVID-19	1. Within 5 days of admission to ICU 2. ±5 days of midpoint of ICU stay 3. Within 5 days of discharge from ICU 4. ≥7 days post-ICU discharge	Illumina MethylationEPIC BeadChip

Supplemental References

1. Mammalian Methylation Consortium, Lu, A.T., Fei, Z., Haghani, A., Robeck, T.R., Zoller, J.A., Li, C.Z., Zhang, J., Ablaeva, J., Adams, D.M., et al. (2021). Universal DNA methylation age across mammalian tissues 10.1101/2021.01.18.426733.

2. Meer, M.V., Podolskiy, D.I., Tyshkovskiy, A., and Gladyshev, V.N. (2018). A whole lifespan mouse multi-tissue DNA methylation clock. eLife *7*, e40675. 10.7554/eLife.40675.

3. Petkovich, D.A., Podolskiy, D.I., Lobanov, A.V., Lee, S.-G., Miller, R.A., and Gladyshev, V.N. (2017). Using DNA Methylation Profiling to Evaluate Biological Age and Longevity Interventions. Cell Metab. *25*, 954-960.e6. 10.1016/j.cmet.2017.03.016.

4. Stubbs, T.M., Bonder, M.J., Stark, A.-K., Krueger, F., Bolland, D., Butcher, G., Chandra, T., Clark, S.J., Corcoran, A., Eckersley-Maslin, M., et al. (2017). Multi-tissue DNA methylation age predictor in mouse. Genome Biol. *18*, 68. 10.1186/s13059-017-1203-5.

5. Wang, T., Tsui, B., Kreisberg, J.F., Robertson, N.A., Gross, A.M., Yu, M.K., Carter, H., Brown-Borg, H.M., Adams, P.D., and Ideker, T. (2017). Epigenetic aging signatures in mice livers are slowed by dwarfism, calorie restriction and rapamycin treatment. Genome Biol. *18*, 57. 10.1186/s13059-017-1186-2.

6. Thompson, M.J., Chwiałkowska, K., Rubbi, L., Lusis, A.J., Davis, R.C., Srivastava, A., Korstanje, R., Churchill, G.A., Horvath, S., and Pellegrini, M. (2018). A multi-tissue full lifespan epigenetic clock for mice. Aging *10*, 2832–2854. 10.18632/aging.101590.

7. Horvath, S. (2013). DNA methylation age of human tissues and cell types. Genome Biol. *14*, 3156. 10.1186/gb-2013-14-10-r115.

8. Hannum, G., Guinney, J., Zhao, L., Zhang, L., Hughes, G., Sadda, S., Klotzle, B., Bibikova, M., Fan, J.-B., Gao, Y., et al. (2013). Genome-wide Methylation Profiles Reveal Quantitative Views of Human Aging Rates. Mol. Cell *49*, 359–367. 10.1016/j.molcel.2012.10.016.

9. Horvath, S., Oshima, J., Martin, G.M., Lu, A.T., Quach, A., Cohen, H., Felton, S., Matsuyama, M., Lowe, D., Kabacik, S., et al. (2018). Epigenetic clock for skin and blood cells applied to Hutchinson Gilford Progeria Syndrome and ex vivo studies. Aging *10*, 1758–1775. 10.18632/aging.101508.

10. Houseman, E.A., Accomando, W.P., Koestler, D.C., Christensen, B.C., Marsit, C.J., Nelson, H.H., Wiencke, J.K., and Kelsey, K.T. (2012). DNA methylation arrays as surrogate measures of cell mixture distribution. BMC Bioinformatics *13*, 86. 10.1186/1471-2105-13-86.

11. Horvath, S., and Levine, A.J. (2015). HIV-1 Infection Accelerates Age According to the Epigenetic Clock. J. Infect. Dis. *212*, 1563–1573. 10.1093/infdis/jiv277.

12. Sadahiro, R., Knight, B., James, F., Hannon, E., Charity, J., Daniels, I.R., Burrage, J., Knox, O., Crawford, B., Smart, N.J., et al. (2020). Major surgery induces acute changes in measured DNA methylation associated with immune response pathways. Sci. Rep. *10*, 5743. 10.1038/s41598-020-62262-x.

13. Guintivano, J., Arad, M., Gould, T.D., Payne, J.L., and Kaminsky, Z.A. (2014). Antenatal prediction of postpartum depression with blood DNA methylation biomarkers. Mol. Psychiatry *19*, 560–567. 10.1038/mp.2013.62.

14. Knight, A.K., Conneely, K.N., Kilaru, V., Cobb, D., Payne, J.L., Meilman, S., Corwin, E.J., Kaminsky, Z.A., Dunlop, A.L., and Smith, A.K. (2018). SLC9B1 methylation predicts fetal intolerance of labor. Epigenetics *13*, 33–39. 10.1080/15592294.2017.1411444.

15. Gruzieva, O., Merid, S.K., Chen, S., Mukherjee, N., Hedman, A.M., Almqvist, C., Andolf, E., Jiang, Y., Kere, J., Scheynius, A., et al. (2019). DNA Methylation Trajectories During Pregnancy. Epigenetics Insights *12*, 2516865719867090. 10.1177/2516865719867090.

16. Smew, A.I., Hedman, A.M., Chiesa, F., Ullemar, V., Andolf, E., Pershagen, G., and Almqvist, C. (2018). Limited association between markers of stress during pregnancy and fetal growth in 'Born into Life', a new prospective birth cohort. Acta Paediatr. *107*, 1003–1010. 10.1111/apa.14246.

17. White, W.M., Brost, B.C., Sun, Z., Rose, C., Craici, I., Wagner, S.J., Turner, S., and Garovic, V.D. (2012). Normal early pregnancy. Epigenetics *7*, 729–734. 10.4161/epi.20388.